Preliminary Characterization of the Altair Lunar Lander Slosh Dynamics and Some Implications for the Thrust Vector Control Design

Allan Y. Lee,[1,*] Alan Strahan,[2] Rebekah Tanimoto,[1] and Arturo Casillas[1]

[1]*Jet Propulsion Laboratory*
4800 Oak Grove Drive, Pasadena, CA 91109-8099
California Institute of Technology

[2]*Johnson Space Center*
NASA Johnson Space Center, 2101 NASA Parkway, Houston, Texas 77058

This paper describes a conceptual design of the Thrust Vector Control (TVC) system and preliminary modeling of propellant slosh, for the Altair Lunar Lander. Altair is a vehicle element of the NASA Constellation Program aimed at returning humans to the moon. Guidance, Navigation, and Control (GN&C) is the measurement and control of spacecraft position, velocity, and attitude in support of mission objectives. One key GN&C function is the commanding of effectors that control attitude and impart ΔV on the vehicle, utilizing both reaction control system (RCS) thrusters and throttling and TVC gimbaling of the vehicle main engine. Both the Altair descent and ascent modules carry fuel tanks. During thrusting maneuvers, the sloshing of liquid fuels in partially filled tanks can interact with the controlled system in such a way as to cause the overall system to be unstable. These fuel tanks must be properly placed, relative to the spacecraft's c.m., to avoid any unstable interactions. Following this will be a discussion of propellant slosh modeling work performed for the present vehicle configuration, including slosh frequency and participatory fluid mass predictions. Knowing the range of slosh mode frequencies over mission phases, the TVC bandwidth must be carefully selected so as not to excite the slosh modes at those frequencies. The likely need to increase the damping factor of slosh modes via baffles will also be discussed. To conclude, a discussion of operations procedures aimed at minimizing TVC-slosh interactions will be given.

[*]Manager, Guidance, Navigation, and Control System, Altair Lunar Lander. Mail Stop 230-104, Jet Propulsion Laboratory, 4800 Oak Grove Drive, Pasadena, California 91109-8099, USA. Allan.Y.Lee@jpl.nasa.gov

Acronyms

ACC	Accelerometer
AL	Air Lock
Altair	Lunar Lander Vehicle
AM	Ascent Module
ARES-I	Launch vehicle for Orion
ARES-V	Launch vehicle for Altair
BOB	Bang Off Bang (an attitude control algorithm)
B/U	Backup
BW	Bandwidth (of a controller)
CAD	Computer Aided Design
CARD	Constellation Architecture Requirement Documents
CEV	Crew Exploration Vehicle
CFD	Computational Fluid Dynamics
c.m.	center of mass
CSI	Control Structure Interactions
DM	Descent Module
DOI	De-orbit Injection (burn)
DRM	Design Reference Mission
DSN	Deep Space Network
EBGS	Earth Based Ground System (DSN tracking complexes plus three other receive-only stations)
EDS	Earth Departure Stage
FFT	Fast Fourier Transformation
FITH	Fire-In-The-Hole
FSW	Flight Software
GN&C	Guidance, Navigation, and Control subsystem
IMU	Inertial Measurement Unit
JPL	Jet Propulsion Laboratory
LEM	Lunar Excursion Module
LEO	low-Earth orbit
LH2	Liquid Hydrogen
Lidar	Light Intensification, Detection, and Ranging
LIDS	Low Impact Docking System
LLO	Low Lunar Orbit
LLV	Lunar Lander Vehicle
LOI	Lunar Orbit Insertion
LOX	Liquid Oxygen
LV	Launch Vehicle
MCC	Mission Control Center Mid-course Correction (Apollo terminology. Same as TCM)
MET	Mission Elapsed Time
MMH	Monomethylhydrazine
mrads	milli-radians (about 0.057296°)
MRO	Mars Reconnaissance Orbiter
MSL	Mars Science Laboratory
NAC	Narrow Angle Camera
NCC	Number, Corrective Combination (Apollo terminology)
NEAR	Near Earth Asteroid Rendezvous
NF	Navigation Filter
NTO	Nitrogen Tetroxide
ONSS	Optical Navigation Sensor System
OpNav	Optical Navigation
Orion	Crew Exploration Vehicle
PAI	Powered Ascent Insertion
PC	Plane Change
PD&L	Powered Descent and Landing
PDI	Powered Descent Initiation
PEG	Power Explicit Guidance
PMD	Propellant Management Device
PRA	Probabilistic Risk Assessment
RCS	Reaction Control System
R/F	Radio Frequency
RPODU	Rendezvous Proximity Operations Docking and Undocking
RSS	Root Sum (of) Squares
SAR	Single Axis Rotation
S/C	Spacecraft
SRU	Stellar Reference Unit (usually called a Star Tracker)
SwRI	Southwest Research Institute
TBD	To Be Determined
TCM	Trajectory Correction Maneuver (same as MCC)
TD	Touchdown
TDRS	Terminal Descent Radar System
THDSS	Terrain Hazard Detection Sensor System
TLC	Trans-Lunar Coast
TLI	Trans Lunar Injection (burn)
TPBVP	Two Point Boundary Value Problem
TPI	Terminal Phase Initiation
TOF	Time Of Flight
TRL	Technology Readiness Level
TRN	Terrain Relative Navigation
TVC	Thrust Vector Control (a ΔV burn performed by a gimbal engine)
VDI	Vertical Descent Initiation
VOF	Volume of Fluid

Table of Contents

Section Page

Acronyms 2
I. Introduction 3
II. Design Reference Mission 4
III. Key Altair Guidance, Navigation, and Control Related Functionalities 6
IV. A Preliminary Altair GN&C System Design 7
  A. GN&C Sensor Suite 8
  B. RCS Thruster Configuration Designs 9
  C. Propulsive Maneuver Control System Designs 11
V. Unstable Interactions between Thrust Vector Control and Sloshing Liquid in Tanks 13
VI. Estimation of Fuel Slosh Mode Frequency 18
  A. Analytical Approaches 19
  B. Computational Approaches 25
VII. Some Preliminary Thought on Altair Thrust Vector Control Design 27
VIII. Operations Considerations 31
IX. Summary and Conclusions 32
Acknowledgements 32
References 33

I. Introduction

The Constellation Program[+] is NASA's response to the human exploration goals set by former President George W. Bush for returning humans to the Moon by 2020. In January 2004, former President Bush announced the new Vision for Space Exploration for NASA. The fundamental goal of this vision is to advance U.S. scientific, security, and economic interests through a robust space exploration program. To this end, the NASA Constellation Program is working on two spacecraft (the Crew Exploration Vehicle named Orion and the Lunar Lander Vehicle named Altair), two launch vehicles (ARES-I will launch Orion and ARES-V will launch Altair), and surface support systems to establish a lunar outpost. This work will provide experience needed to expand human exploration farther into the Solar System. The first crewed flight of the Orion spacecraft is scheduled for no later than 2015, when it will fly to the International Space Station. Altair's first landing on the Moon with an astronaut crew is planned for no later than 2020.

The Lunar Lander Altair is the linchpin in the Constellation Program for human return to the Moon. The Guidance, Navigation, and Control (GN&C) system must perform many functions that are critical to the Altair mission. One key GN&C function will be the commanding of effectors that control attitude and impart ΔV on the vehicle, utilizing both Reaction Control System (RCS) thrusters and throttling and TVC gimbaling of the vehicle main engine. The purpose of this paper is to describe a conceptual design of the Thrust Vector Control (TVC) system and preliminary modeling of propellant slosh, for the Altair Lunar Lander. To this end, key requirements the GN&C system must satisfy, and functions it must perform, in various mission phases will first be described. The Altair GN&C system (including its sensor suite and thruster configurations) that is configured to support these requirements and functions has already been documented[6] and it will only be briefly summarized in this paper. To provide context, a brief description of the current Altair mission timeline with a focus on the various powered flight ΔV maneuvers will be provided. Both the descent and ascent modules of Altair carry fuel tanks. During thrusting maneuvers, the sloshing of liquid fuels in partially filled tanks can interact with the TVC (or RCS thrusters) controlled system in such a way as to cause the overall system to be unstable. Hence, these fuel tanks must be properly placed, relative to the spacecraft's c.m., to avoid any unstable interactions. Following this will be a discussion of propellant slosh modeling work performed for the present vehicle configuration, including slosh

[+]The future of the human space flight program, and thus the Constellation program, is currently being discussed at the highest levels of the U.S. government. For the purposes of documenting the Altair design, this paper is written without consideration of any forthcoming changes in the direction (or even existence) of the program.

frequency and participatory fluid mass predictions. To conclude, a discussion of the TVC system design, with its accommodation of predicted slosh characteristics and overall sensor and structural dynamics, will be provided along with a discussion of operations procedures aimed at minimizing TVC-slosh interaction.

II. Design Reference (Polar Sortie) Mission

Similar to that of the Apollo Lunar Module, Altair is envisioned to be a two-stage vehicle, comprising a Descent Module (DM) and an Ascent Module (AM). Using propulsion elements carried by the unmanned DM, the mated DM/AM will descend from a lunar parking orbit and land on the Moon. Altair will be capable of landing four astronauts on the Moon and of providing life support and a base for weeklong initial surface exploration missions. Using propulsion elements carried by the manned AM, only the AM will ascend from the lunar surface, returning the crew to the Orion spacecraft that will bring them back to Earth. A representative Altair mission profile consists of the following sub-phases:

- Pre-launch ground operations and launch vehicle (LV) boost phases
- LEO operations and mating of Altair/EDS with Orion
- Trans-lunar injection of the mated EDS/Altair/Orion
- Separation of the mated Orion/Altair from EDS
- Trans-lunar coast
- Lunar orbit insertion of the mated Orion/Altair vehicle into a low lunar orbit (LLO)
- Undocking of Altair with Orion in LLO
- Plane change (ΔV) burn
- De-orbit ΔV burn
- Descent and landing
- Lunar surface operations
- Ascent, rendezvous, and proximity operations
- Docking of the ascent module with Orion in LLO
- Control of the mated Orion/AM by Orion GN&C system
- Separation of Altair from Orion
- Disposal of Altair

The mission starts with the use of the ARES-I launch vehicle to insert Orion into a 100-km low Earth Orbit (LEO). Next, the ARES-V heavy-lift launch vehicle will insert Altair, which is mated with the Earth Departure Stage (EDS), into the same orbit. At liftoff, Altair has a mass of 45 metric tons. During docking operations with Orion in LEO, the passive Altair/EDS stack will be controlled by EDS. After spending 2–3 days in LEO, the EDS will be fired to impart 3.1–3.2 km/s ΔV on the mated Orion/Altair vehicle and send it on its way to the Moon. The duration of the trans-lunar injection (TLI) burn is about 6 min. Within 0.5–1 hour after the completion of the TLI burn, EDS will be separated from the mated Altair/Orion. Post-separation, the Altair GN&C system will begin to execute all guidance, navigation, and control functions of the mated Orion/Altair vehicle.

The Trans-lunar Coast (TLC) will last 90–100 hours. During the TLC phase, Altair GN&C will perform four (or more) trajectory correction maneuvers (TCM) in order to keep the spacecraft on a pre-computed reference trajectory. Typically, these are small burns (<30 m/s) that will be executed using RCS thrusters of the Descent Module. The long coast time offers opportunities to perform many checkouts and calibrations of GN&C sensors and equipment. Upon arrival at the Moon, the powerful gimbaled engine of the Altair descent module will be fired for 10–11 minutes in order to slow down the velocity of the stack by 891 m/s. At the end of the lunar orbit insertion (LOI) burn, the gravity field of the Moon will capture the mated vehicle into a 100-km low lunar orbit (LLO). This LLO will be a polar orbit for landing targets that are located near the south pole of the Moon. Table 1 provides a list of discrete propulsive maneuvers that will be executed by the Altair GN&C system.

Table 1. Discrete Propulsive Maneuvers to be executed by Altair GN&C System

Discrete Propulsive Maneuvers	Approximate ΔV Magnitude* [m/s]
Trajectory correction maneuvers (TCM 1-4)	2–22
Lunar orbit insertion (LOI)	891
Plane change (PC)	28.3–28.5
Deorbit Insertion burn (DOI)	19.2–19.4
Powered descent and landing (PD&L)	2074
Powered Ascent Insertion burn	1650–1700
Rendezvous burns:	
Clean-up burn	1–2
Terminal Phase Initiation	19–20
Disposal burn	32–34

*Details are given in Ref. 7.

After spending about one day in the LLO, Altair will undock with Orion. Orion will execute both the undocking and the separation maneuvers. About 1.5 hours after the separation event, Altair will use the DM engine to perform a small (28.3–28.5 m/s) Plane Change (PC) ΔV burn in order to target the Shackleton landing site near the South Pole. The duration of the PC burn is about 19 s. Another 1.5 hours after the PC burn, Altair will use the DM RCS thrusters to perform a small (19.2–19.4 m/s) de-orbit insertion (DOI) ΔV burn. The DOI burn will last about 5.7 min., and Altair has a mass of about 32 metric tons at the end of the DOI burn. The DOI burn will place Altair on an orbit that has a perilune of 15.24 km. At the perilune, the gimbaled engine of the DM will be ignited to initiate the powered descent burn.

Initially, the powered descent burn (2074 m/s) will focus on braking the orbital speed of the vehicle. To do this efficiently, the engine thrust will be closely aligned with the velocity vector of Altair. At an altitude of about 2 km, nearly 3 minutes before touchdown, the Altair will make a large change in its attitude via a "pitch-up" maneuver. In so doing, the guidance algorithm will sacrifice fuel utilization efficiency in order to provide landing-site visibility for both the crew and the terrain hazard detection sensor system. With this attitude change, hazardous terrain features (craters, rocks, and surface slopes with angles too great for the Altair landing gear design) could be identified by both crew members and sensors, and a landing site "re-designation" made, if necessary, to avoid the hazardous landing site. During the final vertical descent of the vehicle, GN&C will focus on achieving a vehicle's touchdown state that is consistent with the landing gear design. Nominally, it will take Altair about twelve minutes, from the initiation of the powered descent burn, to land on the Moon. At the time of touch down, Altair will have a mass of 19-20 metric tons.

After a stay of 5–7 days on the Moon, a series of burns will be executed to bring the Ascent Module (AM), housing the Crew, back to a 100-km LLO where it will dock with the orbiting un-crewed Orion. At liftoff, the Altair AM has a mass of about 7 metric tons. The first burn, named ascent insertion burn, will be executed using the un-gimbaled engine of the AM in three sub-phases. After a vertical rise to achieve an altitude of 100 m, thrusters will be fired to execute a single-axis rotation (SAR) and orient the vehicle attitude to a desirable flight path angle for the next sub-phase. The AM GN&C will then use the Powered Explicit Guidance (PEG) algorithm to complete the insertion burn until engine cutoff. The time of this insertion burn is about 7 min. Nominally, the ascent insertion burn will place AM in a 15.24 km × 75 km orbit. Rendezvous, Proximity Operations, and Docking (RPOD) maneuvers are initiated 10–15 min. after the completion of the ascent insertion burn. These are discrete maneuvers with coasting in between discrete burns. They are relatively small and therefore will be executed using the AM RCS thrusters. The first discrete burn, about 1–2 m/s, will be used to "clean up" any undesirable trajectory dispersions generated by the ascent insertion burn. Next, the larger Terminal Phase Initiation (TPI) burn, about 19-20 m/s, will place Altair on a coasting trajectory to acquire the R-bar at a distance of 2 km from the orbiting Orion with a radial relative velocity.[6,9] Between TPI and the R-bar acquisition, small maneuvers will be used to shape the trajectory and correct any dispersion.

The proximity operations phase consists of many small maneuvers to be executed by Altair, to close the gap between Altair and Orion, in "steps". During proximity operations, the uncrewed Orion will be the passive vehicle,

and its thrusters will be used to maintain the spacecraft in a quiescent state. To achieve a soft docking, Altair will measure the relative angular and translational displacements and rates between vehicles via its docking sensor. The AM thrusters with small minimum impulse bit will then be used to generate the needed small translational and angular rate changes. To achieve a safe docking, the contact conditions between the vehicles must be controlled to levels that are acceptable to the Low Impact Docking System (LIDS). Key contact conditions include the relative translational and angular rates between the mating vehicles as well as the relative translational and angular attitudes, about all spacecraft axes. Altair has a mass of 3.3 metric tons at the time of docking. Measuring from the time of lunar liftoff, the AM will be able to complete the entire process in just less than 3 hours.

After a successful transfer of Crew from the AM to Orion, the crewed Orion will perform the undocking and separation maneuvers to achieve a safe separation distance the vehicle. Before the Crew start their preparations for the Trans-Earth Injection (TEI) burn, they will send commands for Altair GN&C system to execute a second deorbit insertion to "dispose" the AM near a pre-selected site on the Moon. Henceforth, the Orion GN&C system will assume all GN&C responsibilities.

III. Key Altair Guidance, Navigation, and Control Related Functionalities

The Constellation Architecture Requirements Document (CARD) defines requirements controlled by the Constellation Program for hardware, software, facilities, personnel and services needed to perform the design reference missions.[13] The CARD is structured to provide top-level design guidance, architecture wide requirements, and allocations to the systems. A list of key GN&C-related requirements is given in Ref. 6. Based on the current interpretations of these requirements, the following set of GN&C functions is identified:

- Estimate the three-axis attitude and attitude rate of Altair (with respect to an inertial frame), at all times, satisfying a set of attitude determination accuracy requirements.
- Control both the three-axis attitude and attitude rate of Altair relative to their commanded state, at all times, satisfying a set of attitude control pointing accuracy requirements.
- Determine the "state" of Altair (both the three-axis position and velocity vectors) with respect to a reference frame, at all times, satisfying a set of position and velocity determination accuracy requirements.
- Compute maneuvers associated with lunar descent and landing beginning with DOI after the completion of LOI.
- Compute rendezvous maneuvers associated with lunar ascent and RPOD after the completion of the ascent insertion burn.
- Execute fixed or time-varying commanded ΔV burns:
  - Using either the AM or DM RCS thrusters, satisfying a set of RCS maneuver execution accuracy requirements.
  - Using the gimbaled DM engine, satisfying a set of DM engine maneuver execution accuracy requirements.
  - Using the ungimbaled AM engine, satisfying a set of AM engine maneuver execution accuracy requirements.
  - Response to a crew command to terminate a burn in progress.
- Land Altair near the landing site in any lighting condition and without the aid of pre-deployed lunar surface infrastructure, satisfying a pre-selected landing accuracy requirement.
- Function as either the maneuvering or target vehicle while performing RPOD with Orion in LLO.
- Accept both real-time and stored command sequences from either the mission control center or the crew.
- Collect a pre-selected set of GN&C telemetry data and then routed it either directly to the ground, or to an onboard recorder (for later transmission to the ground).
- Provide onboard manual control of flight path, attitude, and attitude rates when the crew can operate the vehicle.
- Detect a GN&C system fault, isolate the root cause of the detected fault, and autonomously reconfigure the GN&C system to restore the affected GN&C functionalities.

The focus of this paper will be on both the use of the gimbaled DM engine to execute the LOI, PC, and PD&L burns, and the use of the ungimbaled AM engine to execute the powered ascent insertion burn (while the AM RCS thrusters are used to control the spacecraft attitude).

IV. A Preliminary Altair GN&C System Design

The lunar lander vehicle Altair is a three-axis stabilized spacecraft. Three-axis stabilized spacecraft are best suited to missions where a high degree of maneuverability is required. Like the Apollo lunar lander designs, Altair consists of a descent module and an ascent module.

The descent module (DM) is the unmanned portion of Altair. It carries the large descent main propulsion engine, and eight propellant tanks. It also carries a set of RCS thrusters (four thruster pods, with four thrusters per pod). The DM also provides structural supports for both the ascent module and the landing gear. The landing gear provide the impact attenuation required to land Altair on the lunar surface, preventing vehicle tip-over at touchdown. The entire descent module will be enveloped in a thermal and micro-meteoroid shield. As depicted in Fig. 1, the radar system and the terrain hazard detection system are mounted on the descent module.

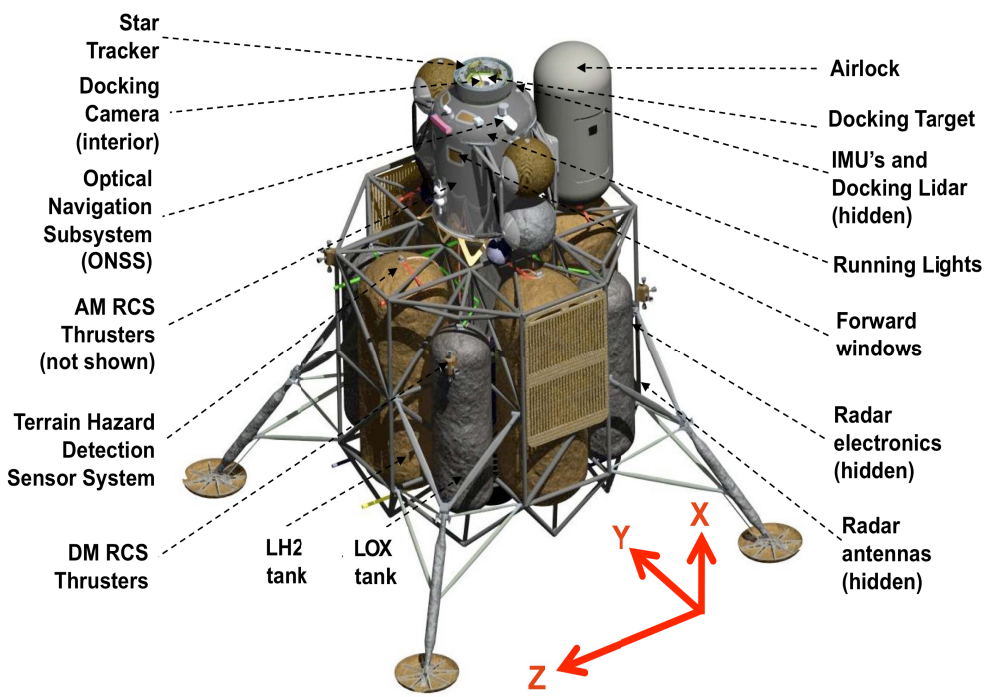

Figure 1. The Altair lunar lander vehicle ("Sortie" lander).[6]

The ascent module (AM) has a crew compartment that provides a controlled environment for up to four astronauts. The sortie lander, depicted in Fig. 1, will carry an airlock for surface EVA. Crews will be in the ascent module at times of lunar landing and docking with Orion. Crew visibility of the landing site will be via the two forward windows. Visibility to Orion at time of docking will be via the two top windows. Near the top of the module is the passive side of the Low Impact Docking System (LIDS) adapter. Three Altair/Orion S-band radio antennas are also mounted near the top of the module. The ascent module carries the ascent main propulsion engine and the associated fuel tanks. It also carries a set of RCS thrusters (four thruster pods, with five thrusters per pod). As depicted in Fig. 1, many GN&C sensors are also mounted on the ascent module.

A. Guidance, Navigation, and Control Sensor Suite

To perform the multitude of GN&C functions listed in Section 3, a set of GN&C sensors is selected. The intent in making this selection was not to promote any particular vendor's sensor or rule out possible use of different sensors in the ultimate spacecraft design, but rather to specify a representative set of sensors that can provide the requisite functionality, based on currently-available technology. The mapping between these GN&C sensors and the functions they support was described in details in Ref. 6. The following paragraphs provide a brief description of the Altair GN&C sensor suite.

The spacecraft's attitude in a celestial frame is estimated using a Stellar Reference Unit (SRU, sometimes called a star tracker) and a set of three gyroscopes. The primary star tracker is mounted on the AM. The backup star tracker, together with a narrow angle camera, are mounted on a 2-dof gimbal platform. This sensor package, named Optical Navigation Sensor System (ONSS), is specifically included in the GN&C sensor suite for the purpose of performing optical navigation.[5] The ONSS can also serve other important GN&C functions. On descent, Altair GN&C plans to use ONSS to perform terrain relative navigation (TRN). This is a navigation technique that takes advantage of known locations of landmarks on the lunar surface. On ascent, the GN&C system plans to use ONSS to perform Orion-relative navigation. In this navigation approach, the range and bearing angles between the two vehicles would be estimated using measurements from ONSS cameras together with supporting onboard software.

Three Inertial Measurement Units (IMU) are included in the Altair GN&C sensor suite. The primary IMU contains four gyroscopes and four accelerometers. The two backup IMU's are identical, and each unit contains three gyroscopes and three accelerometers. If these three IMU's are not co-aligned, and if they are all powered on, independent measurements from 10 gyroscopes and accelerometers will be available. Measurements from three selected prime gyroscopes will be used to support the attitude determination function. Measurements from three selected prime accelerometers will be used to support the propagations of spacecraft's "state" vector (the position and velocity vectors of the spacecraft).[4]

For guidance and control of Altair in the descent and landing phase, a Terminal Descent Radar System (TDRS) will be used to estimate the surface-relative Altair's altitude and velocity. Radars were used on all Mars landers, such as Phoenix. But the specific Altair TDRS is the radar that is being readied for the Mars Science Laboratory (MSL), which will be launched in 2011. The MSL radar uses pulse-Doppler technology to simultaneously provide estimates of altitude and velocity. In the general vicinity of the intended landing site of Altair near the South Pole, there are many terrain hazards that will be challenging to the Altair's landing gear. These hazards include craters, slopes, and rocks. The presence of these types of terrain hazards forced the Apollo-12 crew to make seven re-designations of the landing site before a safe touch down.[17] For the Apollo missions, the identifications of terrain hazards were all made by the crews. This is feasible for well-lighted landing sites that are located within ±20° from the Equator. But even for these missions, near the end of the approach phase of the descent trajectory, crew vision was obscured by the presence of dust clouds. Apollo-11 crews observed dust cloud at an altitude of 30 m.[16] Dust cloud became so intense at 12–15 m that it impaired the visibility of the Apollo-11 crew during the terminal descent and landing phase of the mission. The detection of terrain hazards by crew alone might be risky. For Altair, a sensor named Terrain Hazard Detection System Sensor (THDSS) will be the primary mean of terrain hazard detection.[8] Crew visual detection will be the backup (via out-the-window viewing). Conceptually, THDSS will generate a prioritized list of "hazard free" landing sites and the re-designation to one of these recommended sites will be authorized by the crews.[8]

The rendezvous and docking process consists of a series of orbital maneuvers and spacecraft attitude control motions that successively bring the active vehicle into the vicinity of, and eventually into contact with, the passive vehicle. In low lunar orbit, Altair will be the active vehicle and Orion will be the passive vehicle. Rendezvous and docking is a complex and challenging task, and it must be supported by a set of rendezvous and docking sensors with adequate redundancy. In the current GN&C plan, the bearing angles from Altair to Orion will be estimated using the prime star tracker. As a backup, the cameras of ONSS will be used. The range and range-rate between the two vehicles will be estimated via the two-way S-band radiometric ranging data. Again, as a backup, they could also be estimated using the ONSS cameras. Once the vehicles are within a range of 4–5 km, estimates of the bearing angles and range with better accuracy could be provided by a scanning lidar (Laser Imaging, Detection, and Ranging). Multiple alternative means to acquire these data are available, and lidar was adopted by Altair GN&C only as a placeholder (see Refs. 6 and 9 for details).

B. RCS Thruster Configurations

In collaboration with the Altair Propulsion design team, the GN&C design team designed the RCS thruster configurations on Altair. Altair is equipped with two sets of RCS thrusters, one mounted on the descent module and the other on the ascent module. Both thruster sets use engines that are fed bipropellant fuel monomethyl-hydrazine (MMH) and oxidizer nitrogen tetroxide (NTO). MMH and NTO are hypergolic and have rich space heritage (Galileo, Cassini, Space Shuttle, etc.). For the AM RCS thruster configuration, MMH and NTO are each stored in two tanks. Upstream of these tanks is a high-pressure helium regulation system. The design of the DM RCS thruster configuration is similar. Functions to be performed by the AM and DM thrusters were described in details in Ref. 6 and will be not repeated here. Guided by the identified functionalities (given in Ref. 6), multiple alternative AM and DM RCS thruster configurations were considered. The DM RCS thruster configuration design, depicted in Fig. 2, was selected based on the following selection criteria:

- Minimize the total mass of the thruster configuration
- Minimize the total number of thruster pods
- Minimize the total number of RCS thrusters
- Minimize thruster plume impingement on Altair's sensitive equipment
- Minimize propellant consumption
- Adequate 6-dof control authority in all phases in which the DM RCS thrusters are needed
- Maintain 6-dof control functionality with one arbitrarily failed thruster
- Use thrusters with high TRL
- Use coupled thruster to perform rotational control about all spacecraft's axes

The AM RCS thruster configuration design, depicted in Fig. 3, was selected similarly (though using a different set of selection criteria).

The selected DM RCS thruster configuration consists of four thruster pods, with four thrusters per pod. The plane formed by the thruster pods is located near the predicted center-of-mass (c.m.) location of Altair at the time of touchdown. This arrangement will decouple vehicle's rotational motion from translational motion that will be beneficial to re-designation maneuvers that might be needed just before touchdown. On each thruster pod, there are four 445-N R-4D thrusters. Two thrusters are pointed in the ±X-axis directions. The other two thrusters are pointed ±45° from the ±Z-axis and ±Y-axis (see Fig. 2). Thruster pods are mounted on DM symmetrically while maximizing their moment arms and minimizing interference with the deployment of the landing gear. Rotational control about all spacecraft axes will be performed using coupled thrusters. Thrusts generated by these thruster firings will almost cancel each other, and the ΔV imparted on the spacecraft will be small (but non-zero). This arrangement is important to minimize the size of "non-gravitational" ΔV imparted on the spacecraft.[4] In this early design phase of Altair, plume impingements due to the firings of these DM thrusters are considered acceptable. If needed, thruster "reflectors" will be used to alleviate potential plume-impingement problems.

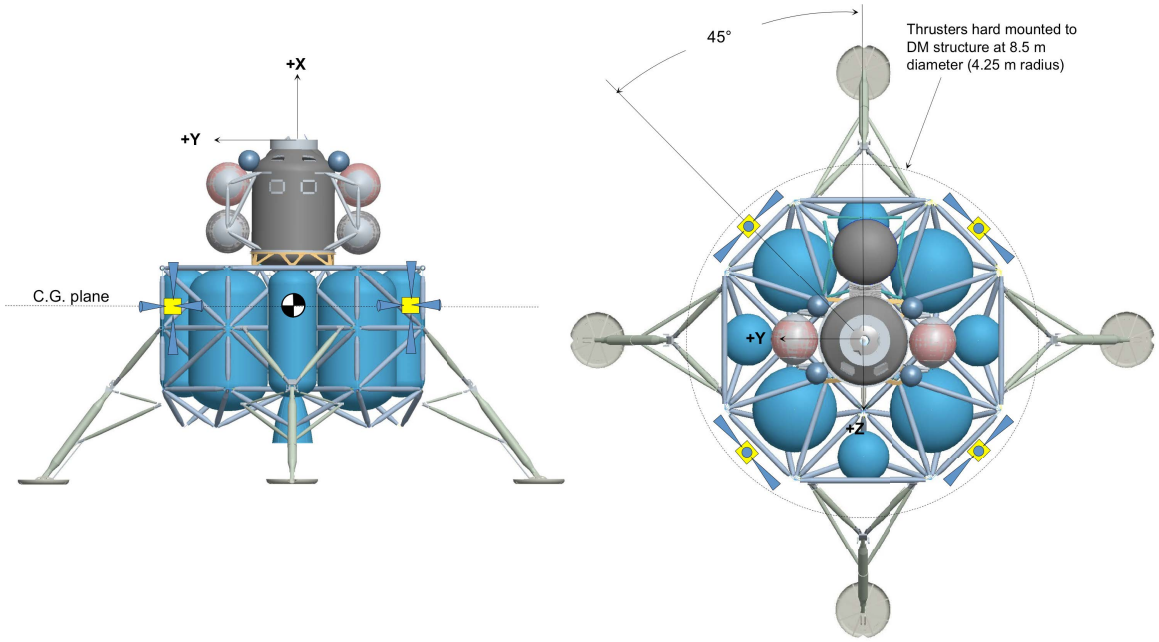

Figure 2. DM RCS thruster configurations

The AM RCS thruster configuration design depicted in Fig. 3 also consists of four thruster pods, with five thrusters per pod. The plane formed by the thruster pods is located near the predicted c.m. location of the AM at the time of docking that will be beneficial to docking controls. This arrangement will decouple vehicle's rotational motion from translational motion. On each thruster pod, there are two 890-N R-42 thrusters (labeled "X" and pointed in the ±X direction), two 22-N *AmPac* thrusters (labeled "D" and pointed ±45° relative to the X-axis), and one 490-N *R-4D* thruster (labeled Y and pointing off the ±Y direction by 30°). Rotational control about all spacecraft axes will be performed using coupled thrusters. This will avoid imparting unwanted ΔV on the spacecraft due to attitude control thruster firing. The 22-N thrusters are needed for docking control. By pointing them 45° away from the X-axis, plume impingement on Orion due to Altair thrusters' firing is minimized.

The AM main engine is not gimbaled. Hence, there will be a need to cant the engine axis through the predicted location of the AM's c.m. at mid-way of the 7-minute burn. The large R-42 thrusters will be used during the ascent insertion burn to counter any tumbling torque imparted on the AM due to canting error, knowledge error of c.m. location, staging torque ("fire in a hole"), etc. Conversely, the small AmPac thrusters will be used during docking operations. In the docking phase, the focus of the GN&C is to meet all the docking conditions dictated by the LIDS mechanism. These docking conditions include bounds on the following relative kinematics between Altair and Orion: in-line and lateral translational closure velocities, angular closure rates about all axes, lateral translational offset distance, and angular misalignments about all axes. These LIDS requirements are stringent and could only be met by the fine control provided by the small thrusters. With the AM RCS thruster configuration, all LIDS docking requirements are met with margins.[9]

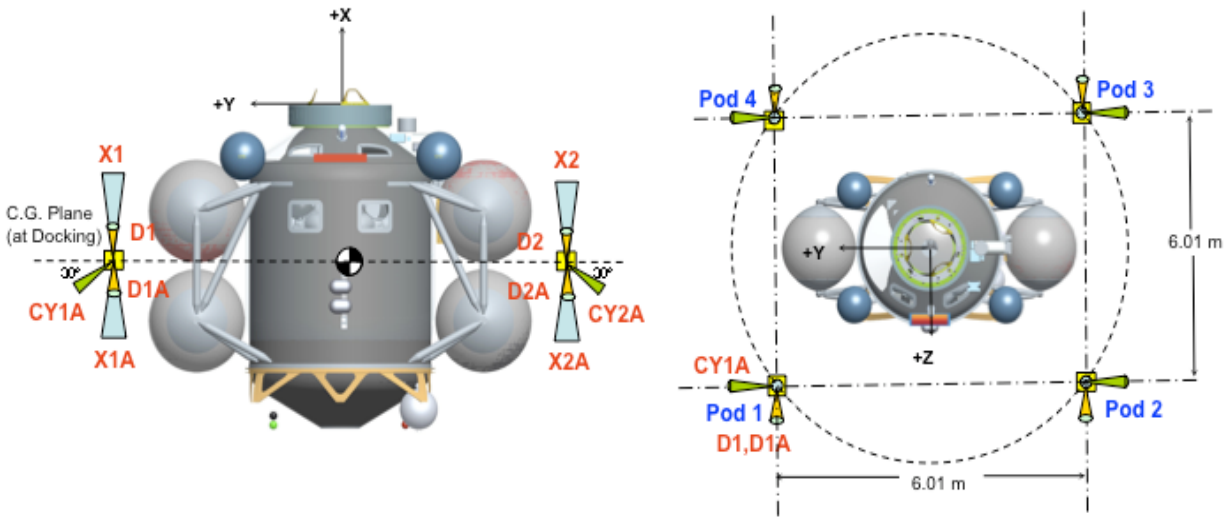

Figure 3. AM RCS thruster configuration.

C. Propulsive Maneuver Control System Designs

Pre-launch, based on the established design reference mission (DRM), navigation analysis and design tools will be used to generate a reference trajectory for the Altair mission. Besides the obvious need to be fuel efficient, the reference trajectory must also meet other requirements such as a capability to execute the undocking maneuver of Altair and Orion (in LLO) in Earth view. The approved reference trajectory will involve the execution of both large and small ΔV burns. Large burns such as LOI (891 m/s) and the powered descent burn (2074 m/s) will obviously be executed using the DM engine. Small burns, such as the trajectory correction maneuvers, will be executed using RCS thrusters. Intermediate size ΔV burns such as the DOI (19.2–19.4 m/s) and PC (28.3–28.5 m/s) could be executed using either engine or thrusters. The merits and demerits of using either engine or thrusters must be established, and decisions made. At times, decisions are made due to other hardware considerations. For example, there might be an upper bound on the number of times the DM engine could start and restart. In the current Altair mission design, we plan to perform DOI using DM RCS thrusters and PC using the DM engine. See Refs. 4 and 7 for details.

Three-axis stabilized spacecraft (such as the Viking Mars orbiter and Cassini Saturn orbiter[3]) had used a two-axis gimbaled engine to successfully and accurately execute their orbit-insertion burns. Altair has adopted this proven approach. In a gimbaled engine burn, Altair's motions about the Y and Z-axis axes are controlled by engine gimbal actuators. In parallel with the gimbal control system, both the Apollo vehicles and the Space Shuttle had used RCS thrusters to form a backup controller (with wide deadbands) in case the TVC control authority is temporarily exceeded. The placeholder Altair TVC controller design will be described in greater details in Section 7. Thrusters will be used to control the Altair's X-axis motion. Band-off-bang controller that is commonly used to control spacecraft attitude such as the one used on the Cassini spacecraft[28] is the placeholder design. Flight experience associated with the Cassini RCS controller design was described in details in Ref. 3. The ΔV imparted on the spacecraft will be measured by the IMU (accelerometer). The burn is terminated once the commanded ΔV is achieved. To this end, flight software will use values of both the scale factor and the bias of the accelerometer that are estimated pre-launch. For better burn accuracy, values of these parameters in the flight software should be updated using values calibrated inflight. A notional schematic diagram of the engine ΔV burn is depicted in Fig. 4.

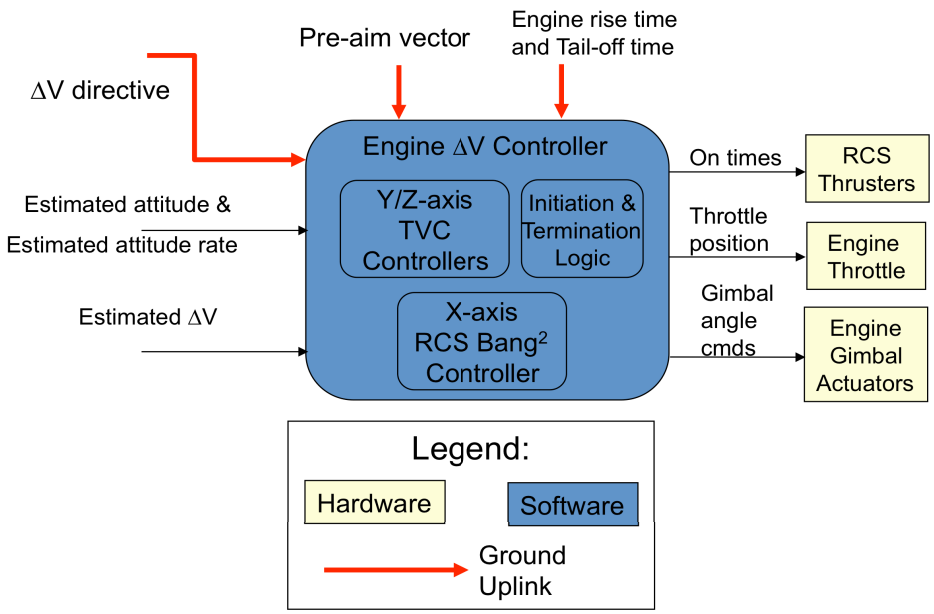

Figure 4. A notional schematic diagram of engine ΔV burn.

Small ΔV's such as the trajectory correction maneuvers will be executed using the X-facing RCS thrusters of either the DM or AM. These burns are called RCS burns. During an RCS burn, the X-facing thrusters are fired to achieve the commanded ΔV. Again, IMU will be used to terminate the burn once the commanded ΔV has been achieved. During an RCS burn, since the vehicle's c.m. is near but not at the exact center of the thruster pods, some thruster off-pulsing will be needed. That is, during an RCS burn, thrusters with (slightly) larger moment arms must sometimes be off-pulsed in order to maintain the Y- and Z-axis motion of the spacecraft within their commanded deadband's. Another set of thrusters will be used to control the X-axis motion of the spacecraft within the commanded deadbands. A notional schematic diagram of the engine ΔV burn is depicted in Fig. 5.

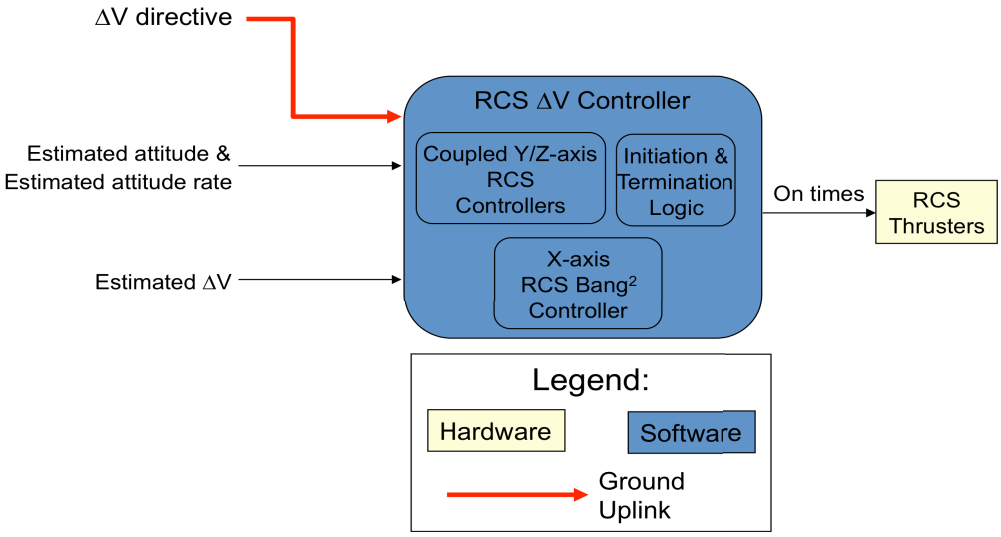

Figure 5. A notional schematic diagram of RCS ΔV burn.

Navigation typically uses a "linear" Gates model[14] to represent propulsive maneuver execution errors. In this model, the ΔV magnitude error ΔV_{Error}^{Mag} is expressed as the sum of a fixed magnitude error e_{Fixed}^{Mag} that is independent of the ΔV magnitude, and a proportional magnitude error e_{Prop}^{Mag} that is proportional to the ΔV magnitude. The fixed magnitude error is typically specified in units of velocity, while the proportional magnitude error is specified in percent. The ΔV pointing error $\Delta V_{Error}^{Pointing}$ is modeled similarly as the sum of a fixed pointing error $e_{Fixed}^{Pointing}$ and a proportional pointing error $e_{Prop}^{Pointing}$ Again, the fixed pointing error is specified in units of velocity while the proportional pointing error is specified in units of angle. The ΔV errors along and perpendicular to the commanded ΔV vector become:

$$\begin{aligned} \Delta V_{Error}^{Mag} &= e_{Fixed}^{Mag} + e_{Prop}^{Mag} \times |V| \\ \Delta V_{Error}^{Pointing} &= e_{Fixed}^{Pointing} + e_{Prop}^{Pointing} \times |V| \end{aligned} \tag{1}$$

In these expressions, |V| represents the magnitude of the ΔV burn.

To control the accuracy of the ΔV burns, Altair GN&C will impose two sets of requirements. One set for all engine burns (e.g., the LOI burn) and another set for burns performed by either DM or AM RCS thrusters. Placeholder Gates requirements are given in Table 2.

Table 2. Placeholder Gates requirements of Engine and RCS ΔV burns.[6]

ΔV Burns	Maneuver Execution Error Requirements (1σ)			
	Fixed Magnitude [mm/s]	Prop. Magnitude [%]	Fixed Pointing [mm/s]	Prop. Pointing [mrad]
Engine	30	0.1	10	3
Thrusters	10	0.1	6	3

V. Unstable Interactions between Thrust Vector Control and Sloshing Liquids in Tanks[6]

Thrust vector stabilization and control is the closed-loop process that keeps the vehicle attitude from tumbling under the high thrust of engine firing and that accepts guidance steering commands to change the direction of the engine-caused acceleration vector. Vehicle motions about the two axes that are perpendicular to the thrust vector are controlled by the gimbal actuators. RCS thrusters are used to control vehicle motion about the remaining axis. Engine throttle is varied to change the magnitude of the acceleration vector. The TVC algorithm will be used to execute three critical ΔV burns of the Altair mission: LOI, PC, and the powered descent burn. A schematic diagram of the TVC is depicted in Fig. 4.

The Altair DM carries eight fuel tanks, four for liquid oxygen (LOX) and four for liquid hydrogen (LH2). During thrusting maneuvers, the sloshing of liquid fuels in partially filled tanks can interact with the controlled system in such a way as to cause the overall system to be unstable. In the post-flight guidance, navigation, and control (GNC) report of the Apollo-11 mission,[16] there were numerous mentions of the impacts of sloshing fuels on vehicle control. For example, during the powered descent phase, the vehicle pitch rate started to diverge near PDI (at 102:36:57 MET). At that time, the peak-to-peak pitch rate was 0.6 °/s. It became 3.0 °/s when MET was 102:39:00. At MET = 102:39:30, the pitch-up maneuver was executed at the start of the approach phase, together with a throttle down and a tightening of deadband (from ±1° to ±0.3°). These control actions arrested the divergence of pitch rate. The peak-to-peak pitch rate dropped from 3.0 to 2.2 deg/s.[16] Experience from the Apollo-11 and other Apollo missions[15,17-18] testified to the need to careful consider the threat of unstable interactions between the TVC and sloshing fuels. To address this threat, the Altair GN&C team studied the following issues in greater depth:

- Placements of fuel tanks relative to the vehicle's c.m.
- Estimation of fuel slosh mode frequency as a function of mission phases.

- Selection of the TVC bandwidth relative to the slosh mode frequencies.
- Use of baffles to increase the damping of the sloshing fuels.
- The inclusion of fuel sloshing models in the dynamics model of the spacecraft used for control design synthesis.

The importance of fuel tank placement is addressed in this Section. To give some insight into the importance of tank placement, we shall consider a simplified rigid spacecraft with a spherical fuel tank, and include the lowest-frequency slosh mode in the dynamic model (cf. Fig. 6).[28] For simplicity, a decoupled single-axis TVC controller will be described in Section 7. Accordingly, only 1-dof pendulum is used in Fig. 6 to represent fuel motion about the S/C's Y-axis. In Fig. 6, the term due to gravity is omitted in this attitude stability study of the spacecraft.

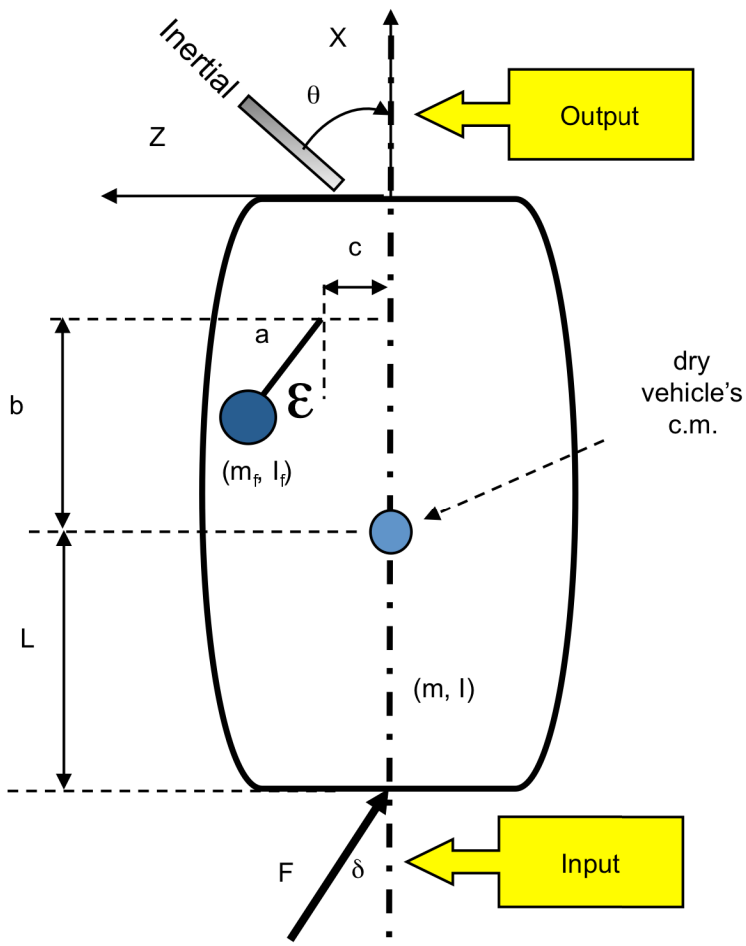

Figure 6. Altair Spacecraft With a Fuel Pendulum.

In Fig. 6, the motion of the sloshing propellant is modeled by an equivalent mechanical pendulum. This approach is similar to those used for the Voyager and Cassini robotic spacecraft.[22–23] This mechanical analog model could mimic, in a gross sense, the reaction forces and moments on the spacecraft from the sloshing propellant. This mechanical analog model is attractive since it allows the TVC control algorithm designers to analyze the interaction between the propellant dynamics and the TVC controlled system. Since the model can be easily implemented in multi-body dynamic simulation models, it could also be used for TVC control system performance verification.

In Fig. 6, the symbols m and m_f denote the masses of the dry spacecraft and the fuel bob, respectively. Here, the word "dry" is used to represent all spacecraft masses that aren't "sloshing". The moments of inertia of the dry spacecraft and fuel are denoted by I and I_f, respectively. The symbols ω and ω_f denote the inertial rates of the dry spacecraft and the fuel, respectively. θ is the attitude of the spacecraft relative to an inertial frame, "a" is the length of pendulum, "b" is the distance between the pendulum pivot point and the S/C's dry c.m., along X-axis, and "c" is the distance between the pendulum pivot point and the S/C's dry c.m., along the Z-axis. The location of the pendulum pivot and the pendulum length will be estimated using techniques to be described in Section 6. Using D'Alembert's principle, equations of motion of the spacecraft and the pendulum bob, as well as relevant kinematics relations could be written. Invoking small angle motions of the spacecraft and fuel bob relative to their trimmed states, the transfer function of the system, from the gimbal angle input (δ) to the spacecraft's attitude (θ) is given by

$$\frac{\theta(s)}{\delta(s)} = -\frac{K}{s^2}\frac{\{1+\frac{s^2}{\Omega_Z^2}\}}{\{1+\frac{s^2}{\Omega_P^2}\}}$$

$$K\ (\sec^{-2}) = \frac{F(L+\frac{m_f}{M}b)}{I+\frac{mm_f}{M}(b^2+c^2-ab)}$$

$$\Omega_Z^2\ (\sec^{-2}) = \frac{aF(L+\frac{m_f}{M}b)\frac{m_f}{M}}{(L+\frac{m_f}{M}b)I_f+\frac{La^2mm_f}{M}} \tag{2}$$

$$\Omega_P^2\ (\sec^{-2}) = \frac{aF\frac{m_f}{M}\{I+\frac{mm_f}{M}(b^2+c^2-ab)\}}{II_f+\frac{mm_f}{M}(I_f(b^2+c^2)+Ia^2)+\frac{m^2m_f^2a^2c^2}{M^2}}$$

$$M = m + m_f$$

To avoid unstable interactions between the TVC and the sloshing fuel, the open-loop "pole" (Ω_P) must be larger than the open-loop "zero" (Ω_Z).[19,28,36] That is, $\Omega_P^2 - \Omega_Z^2 > 0$. It is highly desirable to configure the vehicle to produce a stable interaction between the slosh mode and the spacecraft rigid body mode. An attitude control logic, designed to stabilize the rigid-body mode while neglecting the slosh mode, will naturally stabilize the slosh mode because of such a stable interaction. Using the expressions given in Eq. (2), we can derive the following relations:

$$\Omega_P^2 - \Omega_Z^2 = G\frac{A}{BC},$$

where:

$$G = \frac{aFmm_f^2}{M^2} > 0$$

$$A = -ab(L+\frac{m_f}{M}b)I_f + \frac{a^2bmm_f}{M}\{(-a+b)L-k^2\},\ \text{where } I = mk^2$$

$$B = II_f + \frac{mm_f}{M}(a^2I+b^2I_f) > 0$$

$$C = (L+\frac{m_f}{M}b)I_f + \frac{I\,a^2mm_f}{M} > 0 \tag{3}$$

In these expressions, we note that G and B are always positive. The terms A and B are functions of b, the distance between the pendulum pivot and the dry S/C's c.m. location, along the X-axis. If -L<b<0, both A and C will be positive and $\Omega_P^2 - \Omega_Z^2 > 0$. Accordingly, we will have a stable interaction between the TVC and the fuel pendulum.

That is, the slosh pendulum pivot must be located *below* the dry S/C's c.m. to achieve a stable interaction[6,19,28,36] Performing a similar analysis for a spacecraft with multiple sloshing fuels (the descent module carries eight tanks), one will arrive at the same conclusion. At the end of the 3rd design cycle of the Altair vehicle, the design team has arrived at a vehicle design that is resilience relative to both "Loss of Crew" (LOC) and "Loss of Mission" (LOM) risks. Using the descent module tank geometry, liquid fill level, vehicle's c.m. location, and engine-imparted longitudinal acceleration per that design, the GN&C team generated estimates of the distance between the pendulum pivots and the S/C's c.m. location. From Fig. 7, we note that the condition "b < 0" is satisfied in all mission phases (this is the case as long as red and yellow lines are *below* the blue line). To first-order, there will be no unstable interaction between the sloshing fuels and the TVC controlled system in these mission phases.

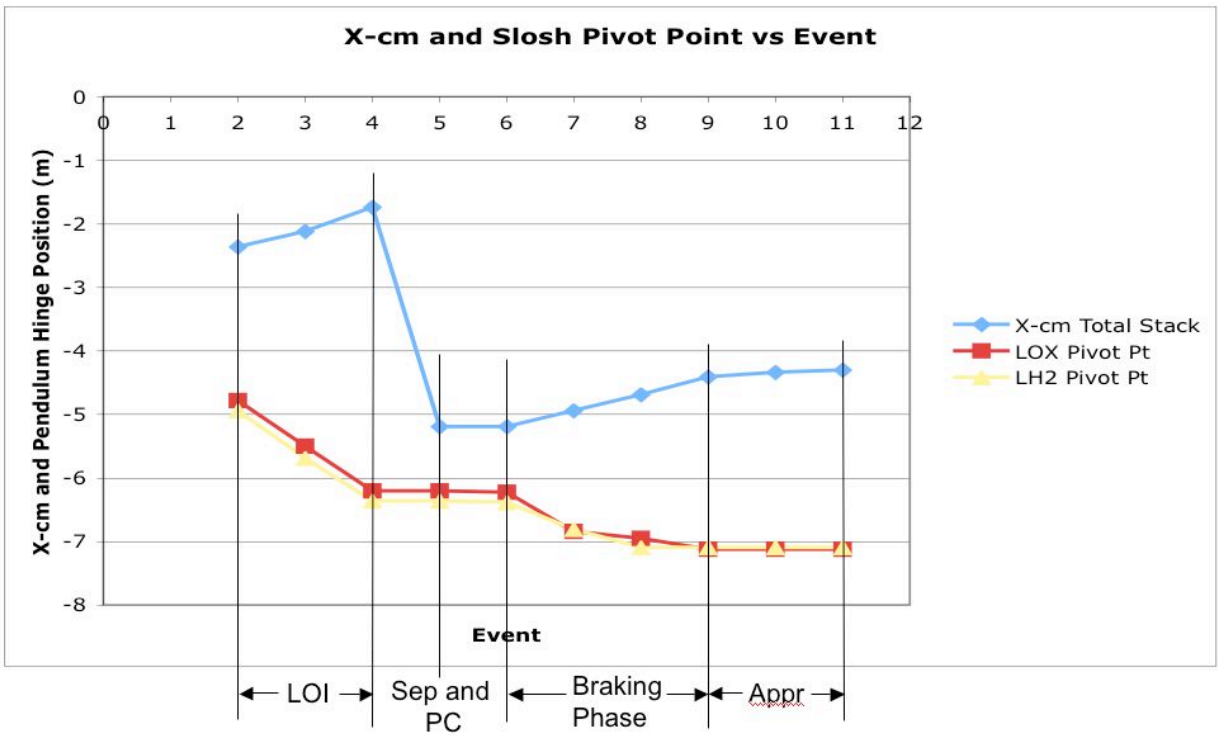

Figure 7. Location of Slosh Pivot Point Relative to Vehicle's c.m.

A similar analysis was made for the powered ascent insertion burn. The AM main engine isn't gimbaled. Hence, there will be a need to cant the engine axis through the predicted location of the AM's c.m. at mid-way of the 7-minute burn. The large R-42 thrusters (cf. Fig. 8) will be used during the ascent insertion burn to counter any tumbling torque imparted on the AM due to canting error, knowledge error of the predicted c.m. location, staging torque ("fire in a hole"), etc. In Fig. 8, the motion of the sloshing propellant (for the ascent insertion burn) is again modeled by an equivalent mechanical pendulum. The symbols m and m_f denote the masses of the dry spacecraft and the fuel bob, respectively. The moments of inertia of the dry spacecraft and fuel are denoted by I and I_f, respectively. The symbols ω and ω_f denote the inertial rates of the dry spacecraft and the fuel, respectively. θ is the attitude of the spacecraft relative to an inertial frame, "a" is the length of pendulum, "b" is the distance between the pendulum pivot point and the S/C's dry c.m., along X-axis, and "c" is the distance between the pendulum pivot point and the S/C's dry c.m., along the Z-axis. The motion of the spacecraft about the [Y,Z] axes will be controlled by four pairs of 890-N thrusters (that are labeled "X" in Fig. 8. See also Fig. 3). The effective magnitude of these thrusters are denoted by "f" in Fig. 8. The positions of these thruster pods are located at [r, h] m from the S/C's c.m., along the [X,Y] axis, respectively. Using D'Alembert's principle, equations of motion of the spacecraft and the pendulum bob, as well as relevant kinematics relations are written. Invoking small angle motions of the spacecraft and fuel bob

relative to their trimmed states, the transfer function of the system, from the RCS thruster couple (f) to the spacecraft's attitude (θ) is given by Eq. (4).

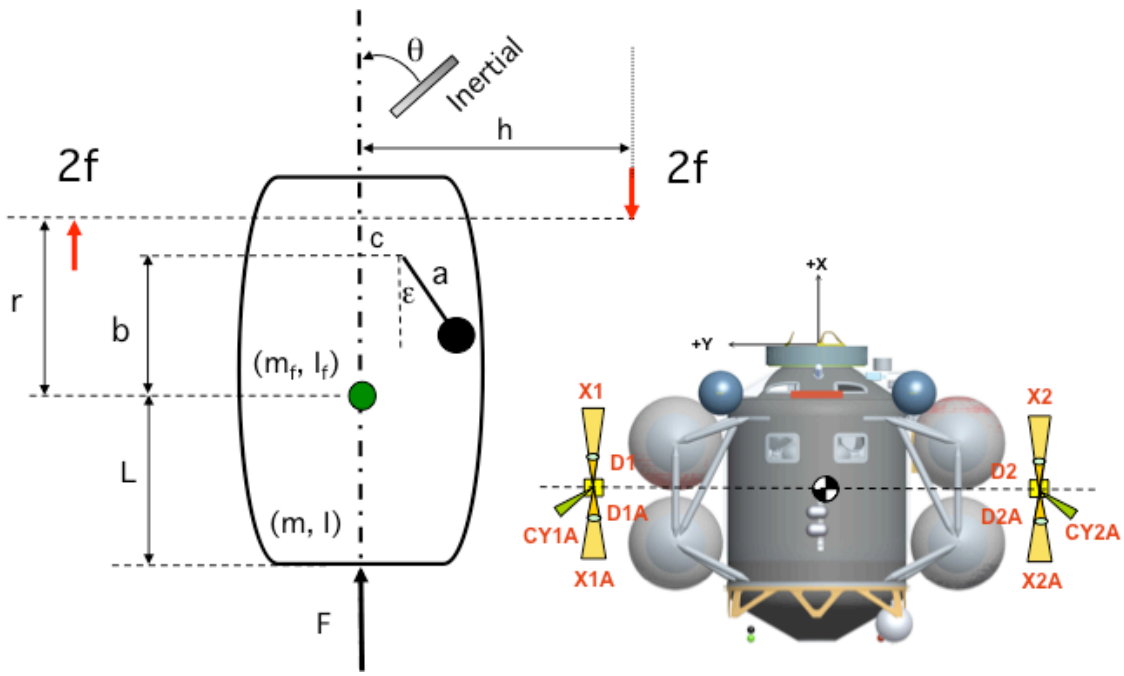

Figure 8. Altair Ascent Module With a Fuel Pendulum.

$$\frac{\theta(s)}{f(s)} = -\frac{K}{s^2}\frac{\{1+\frac{s^2}{\Omega_Z^2}\}}{\{1+\frac{s^2}{\Omega_P^2}\}}$$

Control effectiveness parameter = Gain factor =

$$K\ (kg^{-1}m^{-1}) = \frac{4h}{I+\frac{mm_f}{M}(b^2+c^2-ab)} = \frac{4h}{I} \quad \text{(if } m_f \text{ is very small)} \tag{4}$$

$$\Omega_P^2\ (sec^{-2}) = \frac{m_f aF}{M}\left[\frac{I+\frac{mm_f}{M}(b^2+c^2-ab)}{II_f+\frac{mm_f}{M}\{(b^2+c^2)I_f+Ia^2\}+\frac{m^2m_f^2}{M^2}a^2c^2}\right] > 0$$

$$\Omega_Z^2\ (sec^{-2}) = \frac{\frac{m_f aF}{M}}{I_f+\frac{mm_f}{M}a^2} > 0$$

$$M = m + m_f$$

Again, to avoid unstable interactions between the RCS control system and the sloshing fuel, the open-loop "pole" (Ω_P) must be larger than the open-loop "zero" (Ω_Z). That is, $\Omega_P^2 - \Omega_Z^2 > 0$. Using the expressions given in Eq. (4), we can derive the following relations:

$$\Omega_P^2 - \Omega_Z^2 = G\frac{A}{BC},$$

where :

$$\begin{aligned} G &= \frac{am_f F}{M} > 0 \\ A &= \frac{mm_f}{M}ab\{\frac{mm_f}{M}a(b-a) - I_f\} > 0 \text{ if } b < 0 \\ B &= II_f + \frac{mm_f}{M}\{(b^2+c^2)I_f + Ia^2\} + \frac{m^2m_f^2}{M^2}a^2c^2 > 0 \\ C &= I_f + \frac{mm_f}{M}a^2 > 0 \end{aligned} \tag{5}$$

In these expressions, we note that G, B, and C are always positive. The term "A" is a function of the distance between the pendulum pivot and the dry S/C's c.m. location, along the X-axis. It is positive if b<0, and we will have a stable interaction between the RCS controller and the fuel pendulum. Accordingly, to first order and just like the placements of DM tanks, the slosh pendulum pivot of AM fuel must be located *below* the dry S/C's c.m. to achieve a stable interaction between the RCS thruster control system and the sloshing fuels during the powered ascent burn. Once "b" is computed for the current Altair AM design, we will know whether there is a need to change the locations of the fuel tanks in order to achieve a stable interaction between the sloshing fuel and the RCS controlled system throughout the ascent insertion burn.

VI. Estimations of Fuel Slosh Mode Frequencies

Altair is a flexible spacecraft and the design of the TVC system must consider these flexibilities. Also, the large quantities of propellants that are needed to perform the ΔV burns are stored in multiple tanks. When the spacecraft experiences high acceleration due to the firing of the descent (or ascent) engine, the poorly damped sloshing motions of the liquid fuel inside the tanks must also be considered in designing the TVC system. Else unstable interaction between the TVC control actions and sloshing motions might occur, leading to degraded performance or even a total vehicle failure. For example, during the powered descent phase of Apollo-11, the magnitude of pitch rate oscillations diverged beginning at the "Window-up" maneuver.[16] Also, during the Trans-Earth Injection burn of Apollo-11, the pitch slosh oscillation persisted throughout the entire Service Module burn. Significant interactions between the sloshing liquids and the TVC system will degrade the maneuver execution performance (magnitude and pointing accuracies) resulting in excessive propellant usage. The loss of the ATS-V (1969)[1] and the Intelsat IV spacecraft (1977)[2] were both attributed to more extreme examples of maneuvering spacecraft slosh interaction. Unstable interactions between sloshing fuel and the TVC system of the NEAR spacecraft also significantly impacted the performance of a critical engine burn.[11] Other spacecraft failures from fuel slosh were documented in Ref. 39.

In order to design a TVC system accommodating slosh, an understanding of expected slosh behavior is required. To this end, simple closed-form analytic and more rigorous computational slosh models have been developed for the Altair Liquid Oxygen (LOX) and Liquid Hydrogen (LH2) propellant tanks. As slosh characteristics are highly dependent on tank geometry, fill level, and overall longitudinal acceleration, the Altair vehicle and tank geometry of the 3rd Altair design cycle, along with mission profile was assumed. Slosh characteristics that affect slosh-TVC interaction and that were modeled for this analysis include (i) lateral slosh frequency, (ii) fluid participatory mass and as the sloshing fluid was modeled as a simple pendulum, (iii) the location of the vehicle center of mass relative to the slosh pendulum pivot point. Sections VI.A and VI.B provide estimates of these slosh model parameters using two alternative approaches, as well as provide some insight into the dynamics of slosh, its modeling, the estimation of liquid damping and how it compares for different fluids.

A. Analytical Approaches

For the analytic modeling of slosh during an acceleration event such as a propulsive ΔV maneuver, the primary slosh motion of interest is typically assumed perpendicular, or in a *lateral* direction, as compared to the *longitudinal* acceleration vector imparted by the propulsive system.[24,33-34] During an acceleration (propulsive) event and due to the relatively low damping of typical liquid propellants, the slosh motion can manifest itself as a lateral oscillatory response to any impulsive disturbance that has a lateral component. For example, the side force of a gimbaling main engine. Even a rotational disturbance due to firings of RCS thrusters could impart a lateral oscillation due to the presence of tank's internal constraints on the motion of the liquid.

There are two common closed form analytic methods for modeling the lateral oscillatory slosh behavior of a liquid in a tank experiencing acceleration. One approach is to model the participating liquid as a lump or body of mass attached to a tank wall via a spring and damper. This is a simplifying approach that constrains the fluid motion to one degree of freedom. Another approach is to model the participating liquid as a mass on the end of a pendulum, allowing multiple degrees of freedom (cf. Figs. 6 and 8). The focus is on the lateral direction with the pendulum oscillating around the predominant acceleration vector.[24,33-34] Each method has advantages though the pendulum approach is adopted by the Altair GN&C team as it was used both for the original Apollo slosh analysis as well as for Cassini work.[2,23,26] Additionally, the pendulum approach has the advantage that the lateral response derives directly from the imparted longitudinal acceleration whereas the spring-mass approach requires a unique calculation of the spring constant for each acceleration level. Furthermore, in the *pendulum* approach, the 'micro-g' terms of the slosh pendulum model could be ignored as they are significant only for very small accelerations typical of a spacecraft venting on-orbit. Generally these terms are several orders of magnitude less than 1 Earth g, and require additional modeling terms to represent fluid surface tension of the liquid of interest.[24] The powered flight maneuvers that are the focus of our slosh analysis have accelerations in the range of 0.15-0.3 Earth g's (see Table 3).

Table 3. Fill fractions and accelerations for key Altair mission profile events

Event[#]	Scenarios	Fill Fraction	Earth G's
2	Start LOI	0.90	0.15
3	Mid LOI	0.70	0.15
4	End LOI	0.50	0.15
6	Start PDI	0.50	0.25
7	Mid PDI	0.28	0.30
8	1/4 burn to go	0.17	0.32
9	Start Approach	0.05	0.17
11	Touchdown	0.03	0.17

[#]See also the caption of Fig. 9.

From the pendulum analytic slosh model, three slosh parameters emerge that support slosh-control system interaction analysis. These slosh parameters are the slosh frequency, participatory mass, and effective pivot point. Arguably the most important of these parameters is the estimated natural frequency of the sloshing liquid, which is derived from estimated pendulum length (see Eq. (6)) and which the thrust vector control system should avoid exciting. The participatory mass, being the amount of liquid that is sloshing in the pendulum model, is important as it correlates to how much force the vehicle experiences and whether flight control would attempt to counter it.[24,33-34] The effective pivot point is the rotation point of the pendulum. As discussed in Section V, there is a strong preference to have the pivot located *below* the rigid body vehicle's c.m. for increased overall system stability.[19,28]

All three slosh pendulum parameters are functions of tank geometry including size, tank fill level, and the longitudinal acceleration imparted on the tank. Interestingly these three slosh model parameters, of interest to flight control, are not a function of the specific liquid being excited, except in that the participatory mass is a fraction of the total fluid mass and is therefore a function of the specific liquid density.[24,33-34] However the damping of the sloshing liquid, which factors into baffle sizing and design,[34] along with the liquid surface tension, if modeling slosh for a micro-g acceleration, do correlate to the specific liquid type.[24]

Literature describing the analytic calculations of these slosh model parameters includes a classic Apollo era NASA publication, SP-106,[33] and an updated version of this same treatise by Southwest Research Institute (SwRI)[24]

along with other supportive publications.[25,34] These references describe analytic techniques for estimating the three slosh parameters for a variety of basic tank shapes including spherical and upright cylindrical. The tank shapes for the original Lunar Excursion Module (LEM), as well as the tank configurations of Altair, are actually a combination of these basic shapes, effectively consisting of upright cylindrical tanks with hemispherical dome caps on the top and bottom. To address this configuration, slosh modeling for the LEM tanks utilized a hybrid approach where if the liquid fill fraction is in either end cap, fuel sloshing motion is modeled using a spherical tank equivalent in size to the hemispherical end cap. If the liquid fill fraction is in the cylindrical portion of tank, one uses an equivalent cylinder with cross sectional area equal to the actual cylinder, but with height sufficient to equal the total tank volume. For spherical tank model, slosh pivot is fixed at the center of the sphere. For cylindrical tank model, the slosh pivot point translates along the longitudinal axis as function of fill level.[26] This approach was adopted for analytic modeling of slosh motions inside the Altair's propellant tanks. The Altair's descent module carries four identical LOX tanks, and four identical LH2 tanks. All eight tanks are upright cylinders with hemispherical end caps. Relative to the LOX tanks, the LH2 tanks are slightly taller and significantly larger in diameter (due to the low density of liquid hydrogen).

It is assumed that single or multiple tanks would have the same basic slosh characteristics as these are only a function of tank size and geometry. It is also assumed in calculating total participatory slosh mass for the vehicle that the liquid of all the tanks acts together as this would generate a worse case slosh force on the vehicle. If the individual slosh masses of the tanks acted counter to each other, then the overall force on the vehicle would effectively be less. However, no further investigation into multi-tank interaction was pursued in our work. As the Altair vehicle design matures further, it would be recommended that such interactions be explored both experimentally and in simulation, modeling each tank individually with a slosh pendulum model.

A.1 Slosh modeling for basic tank shapes

The specifics of pendulum slosh modeling for a sphere and an upright cylinder, which can then be combined in the hybrid approach just described, are defined in the SwRI reference on slosh modeling. They are briefly reviewed in this paper. Not included here are their derivations, though those also exist in the reference.[24] For a simple spherical tank, a plot of the pendulum length over tank radius, as a function of fill level for the first slosh mode is given in Ref. 24. In the same reference is the participatory mass fraction as a function of fill level for non-sloshing mass as well as the sloshing mass. Once pendulum length and the longitudinal acceleration is defined for a given tank geometry and fill level, the natural slosh frequency (in rad/s) can be estimated with the simple generic pendulum equation:

$$\omega = \sqrt{\frac{a_X}{L}} \tag{6}$$

where L is pendulum length and a_X is the longitudinal acceleration. For the spherical tank, the center of pendulum rotation is assumed to be the center of the tank.[24]

For the upright cylindrical tank, pendulum length, participatory mass and pendulum pivot point, relative to the center of mass of the current total fluid volume, are also given in Ref. 24 as a function of fill level. Again the slosh frequency is calculated from the pendulum length and the longitudinal acceleration using the generic pendulum equation (Eq. (6)).

Though not evident from just reviewing the empirical plots and equations given in Ref. 24, it is worth noting that in general the cylindrical tank has better slosh characteristics (for avoiding flight control interaction) than spherical tank. Specifically, the cylindrical tank when compared to a spherical tank of equal volume has a higher slosh frequency, allowing for more separation from the TVC bandwidth (BW). Details on the importance of having good separation between the TVC BW and slosh frequencies are given in Section VII. The cylindrical tank also has less participatory mass than that of a spherical tank of equal volume. Both of these advantages are due to the smaller exposed liquid surface area within the tank which reduces the amount of liquid that can rise up or down in a slosh wave.[24]

A.2 Slosh modeling for the Altair's *Clean* Tanks

Slosh model parameters were estimated for both the LOX and LH2 tanks for various mission events. They were estimated assuming the latest vehicle mass properties, tank sizes, and tank placements on the vehicle. All slosh frequencies reported here correspond to Altair's *clean* tanks even though, as explained in section VI.A.3, it is highly likely that these tanks will be retrofitted with baffles. Three propulsive events of special interest are the LOI, PC, and PD&L burns. The Lunar Orbit Insertion (LOI) maneuver is a large burn executed by Altair vehicle main engine and TVC acting upon the total vehicle stack of Altair and Orion. About one day after LOI, Altair is separated from Orion. The Plane Change (PC) burn again uses the Altair main engine and TVC but is a relatively short burn acting only on Altair. The last major burn executed by the Altair main engine, requiring TVC, is the Powered Descent and Landing (PD&L) burn. This burn could be divided into three sub-phases. The *braking* phase is where most of the vehicle's orbital velocity is negated, along with a significant reduction in propellant. The *approach* phase begins about one km and about 107 s from the landing area. This phase, included primarily for astronauts to observe the landing area, is immediately preceded with a pitch up of the vehicle, allowing for crew visibility, and a throttle down, allowing for the vehicle to continue to descend in the low lunar gravity. The last phase is the vertical descent and ended with a soft touch down. In this phase, the descent engine will be throttled to maintain a constant vertical vehicle velocity of about 1 m/s before touch down. Details are given in Ref. 6.

Also critical to the estimation of slosh characteristics is the longitudinal acceleration experienced by the vehicle and tanks as this is the forcing function driving energy into the slosh pendulum. Increased acceleration will result in a higher slosh frequency (cf. Eq. (6)). The estimated values of longitudinal accelerations in various mission phases are listed in Table 3.

Fig. 9 shows both LOX and LH2 slosh frequencies (in Hz) versus mission event. Note that the LH2 frequencies are observed to be lower for all mission phases. This is due to the fact that its tanks are significantly larger than the LOX tanks, allowing for more exposed surface area and hence a longer pendulum arm. Estimated frequencies are also observed to be relatively unchanged for events 2–4. This is also true for events 6–8 because the propellant was in the cylindrical portion of the tank (where slosh frequency isn't a strong function of fill level). Frequencies for event 4 (prior to separation of Altair and Orion) and event 5 (PC ΔV burn after separation of Altair and Orion) are about the same even though the vehicle mass was greatly reduced after the separation event. This is the case because the throttle for the PC burn was reduced. The frequencies at event 6 (start of the PD&L phase) are higher than event 5, even with essentially the same mass. This is because of the higher engine throttle (and hence longitudinal acceleration) to be used for event 6. Slosh frequencies are lower for events 9–11 as the throttle has been reduced (see Table 3, from 0.32 to 0.17 Earth's g) and as the propellant gets into the lower end cap where even though the exposed surface area is reducing, the effective pendulum arm is increasing as the pivot point of the arm remains at the radial center point of the lower end cap.[24]

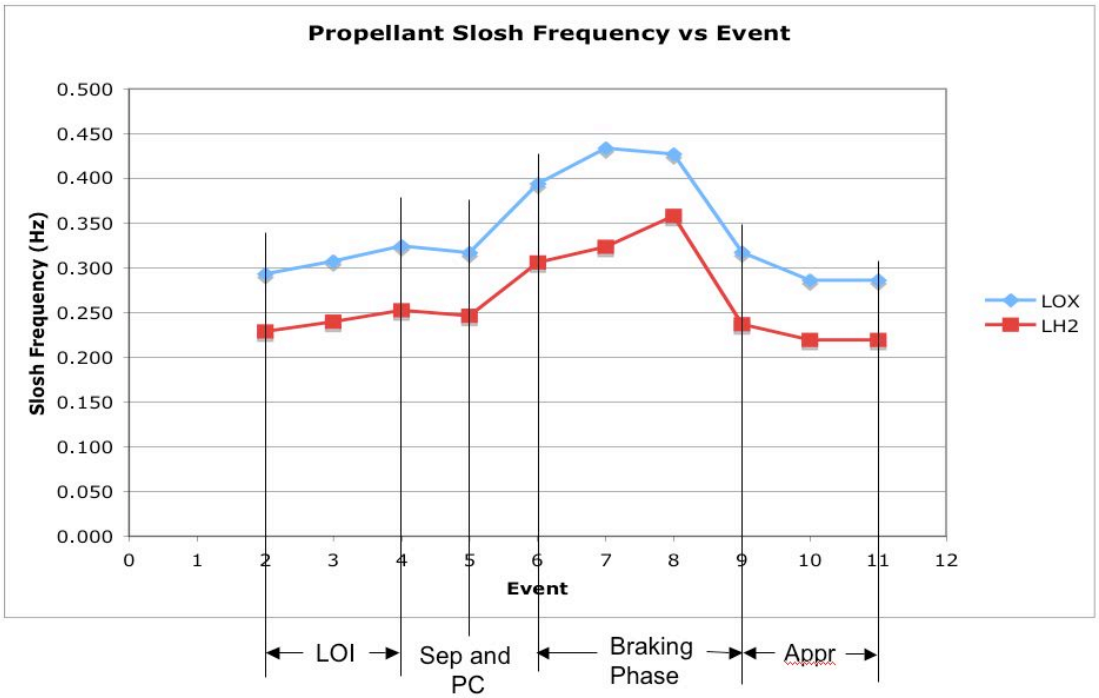

Figure 9. Estimated LOX and LH2 slosh mode frequencies as functions of mission phases.

(1=Post TLI, 2=Start LOI, 3=Mid LOI, 4=LOI completed, 5=Post separation (plane change), 6=Start PD&L, 7=Mid braking burn, 8=1/4 braking burn to go, 9=Start Pitch-up and Approach, 10=Final Descent, and 11=Touchdown)

The estimated range of Altair slosh mode frequencies, 0.21–0.44 Hz, is compared briefly with those of the Saturn orbiter Cassini[3] and the Mars Reconnaissance Orbiter (MRO).[37] The propulsion module of Cassini houses two cylindrical tanks with hemispherical end domes. These tanks each contain an eight-panel Propellant Management Device (PMD) of the surface tension type.[23] These PMD's are used to control the orientation of the propellant in the low-g environment via surface tension forces. In Ref. 3, the power spectrum of the per-axis spacecraft's attitude rates at the time of Saturn Orbit Insertion (when the tanks were about 50% full) were used to estimate the slosh mode frequencies and other spacecraft's structural appendages. The estimated values of the first and second slosh mode frequencies of Cassini were found to be 0.074 and 0.18 Hz, respectively. The MRO spacecraft uses almost identical propellant tanks with similar PMD's. The first slosh mode frequency was determined using Mars Orbit Insertion data and it was found to be 0.23 Hz.[37]

Fig. 10 shows both the LOX and the LH2 slosh participatory mass (assuming all four LOX or all four LH2 tanks slosh and oscillate in unison) versus mission event. The participatory mass of the LH2 is observed to be significantly lower simply because the overall mass of liquid hydrogen required for performing the ΔV maneuvers is much lower. Participatory mass is observed both for the LOX and LH2 to be at a maximum for events 2–6 when in the upper half of the cylindrical portion of the tanks. Participatory mass is not a function of acceleration so there is no variation observed with throttle or vehicle mass changes. The participatory mass begins to drop off as the fill level gets into the lower portion of the cylindrical section and then into the hemispherical cap, as generally expected from the characterizing equations.[24]

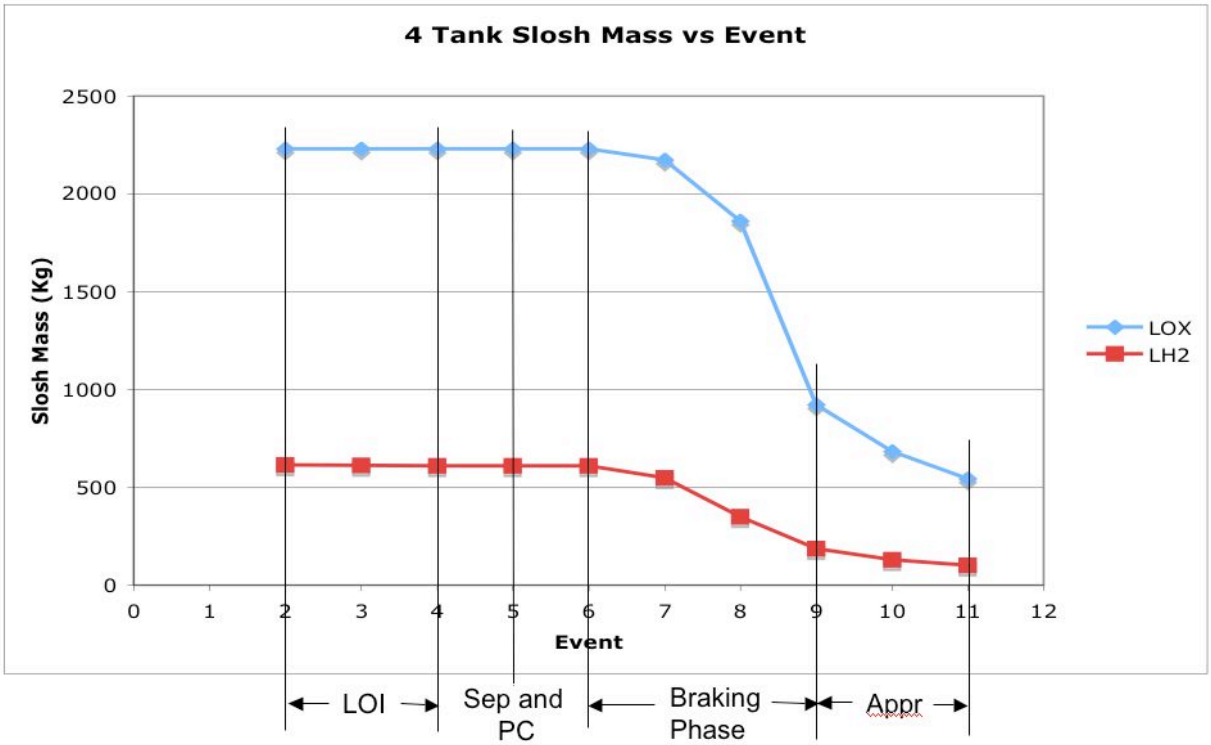

Figure 10. Total Participatory Slosh Mass versus Mission Event

The estimation of the slosh pivot point is shown in Fig. 7 (in section V) where the inherent stability of this fluid and tank geometry is explored. This shows the pendulum pivot point to always lie below the vehicle's c.m., as desirable.[19] This margin was at a minimum (but it is still >1 m) for events 5 and 6, after the Orion had separated, causing the overall stack CM to drop towards the effective pivot point. But, after event 6, the PD&L burn started to consume propellant causing the vehicle's c.m. to rise again (as there was less mass in the tanks to pull the vehicle's c.m. down).

Overall, the events of most interest regarding slosh are events 2–6, where participatory mass is highest, and events 9–11, where vehicle maneuvering could be most significant. Events 5 (the PC burn) and 6 (start of the PD&L burn) are of concern as the participatory mass is the highest. Also, at the start of the PD&L phase, the TVC-controlled high thrust vector of the descent engine might not have pointed through the vehicle's c.m. closely. The resultant ignition transient will likely excite the propellant. However, performing the PC ΔV burn before the PD&L burn will help to locate the vehicle's c.m. location (see section VIII). The on-board knowledge of the vehicle's c.m. location could be used to better pre-aim the descent engine's thrust vector. Events 9–11 (Approach and Vertical Descent to landing sub-phases) are of some concern because the overall slosh natural frequency is lowest, possibly very close to the TVC bandwidth. This is also the time when the vehicle is expected to execute some demanding rotational and translational maneuvers to perform a target re-designation or to accommodate human piloting commands. But the participatory slosh masses in these phases will be very low (cf. Fig. 10).

A.3 Slosh Damping

As stated above, damping of a slosh oscillation is one slosh parameter that does vary with the specific fluid involved, in addition to tank geometry, fill fraction, and longitudinal acceleration.[34] Damping of sloshing liquids is of particular interest as it factors into decisions of how to physically mitigate potential unstable interactions between sloshing propellant and TVC control actions. In particular, whether baffle should be added to tanks and how to size

them.[34] This could be the case if there is inadequate separation between the slosh frequency and the TVC bandwidth, or if maneuvers, especially piloted maneuvers, could excite the slosh mode.

Estimating the damping ratio (ξ) of a sloshing liquid in a smooth walled tank is an inexact science. However, some empirical equations have been derived to provide first-order estimates. For an upright cylindrical tank, similar to that of the current Altair configuration and with a fill level greater than its diameter, the damping ratio could be estimated via the following expression.

$$\xi = 0.79\sqrt{\frac{\nu}{\sqrt{a_X L^3}}} \tag{7}$$

Here, ν (in m^2/s) is the liquid's kinematic viscosity, L (in m) is the tank radius, and a_X (in m/s^2) the longitudinal acceleration.[24] The kinematic viscosity is itself an insightful parameter to calculate for a liquid. It basically represents the tendency of a fluid in motion to damp itself based on its density (correlating loosely to momentum) and dynamic viscosity (correlating loosely to friction).[24] Damping ratios of various sloshing liquid propellants in an 1-m (radius) cylindrical tank and assuming 0.30 Earth's g longitudinal acceleration, similar in size and acceleration to the current lander design and trajectory (see also Table 3), are computed using Eq. (7) and compared in Table 4. These damping values are quite small due in part to the very large tank geometry being considered for the Altair vehicle. Also, it is evident from this table that the propellants chosen for Altair have less damping than those used for the Apollo LEM. That is, with an equivalent impulse or slosh excitation, an Altair propellant will oscillate or 'ring' longer than its Apollo counterpart. Additionally, if slosh excitation can not be prevented outright via sufficient frequency separation from the controller bandwidth, as further discussed in section VII, then it is evident that these fluids will likely require baffles or other slosh mitigation as their estimated damping ratios are almost two orders of magnitude less than that suggested for slosh suppression, being 1–3%.[24,26,34] For comparison, the damping ratio of the MRO fuel slosh mode was estimated to be about 1%.[37]

As it appears the current lander design will require slosh mitigation, a preliminary baffle design has been incorporated into the LOX tanks, where most of the participatory slosh mass would exist, with 3 horizontal ring baffles at locations ranging from near mid tank down to near the feed-line drain. As the Lander design matures, the baffle design would also be refined, possibly with additional baffles being added higher in the LOX tank, and possibly with baffles being incorporated into the LH2 tanks.

Table 4. Estimated Slosh Damping Ratio of Various Liquids in A *Clean* Cylindrical Tank

Liquid	Application	Damping Ratio [%]	Relative to Water [-]
Water	Reference	0.0604	1.00
Aerozine-50	Apollo fuel#	0.0576	0.95
N2O4	Apollo and Shuttle oxidizer#	0.0323	0.53
MMH	Shuttle OMS and RCS fuel	0.0597	0.99
LH2	Altair fuel	0.0258	0.43
LOX	Altair oxidizer	0.0265	0.44
CH4	Alternative Altair fuel	0.0308	0.51

#Estimated values of achieved damping ratios of Apollo fuel slosh modes (with baffles) are on the order of 0.1–0.16%.[30]

B. Computational Approach

It is common practice to determine tank slosh parameters either through a simplified analytical model, when the tank geometry is simple and well-understood, or through a laboratory experiment, when the geometry is more complex or includes internal structure that is not well understood analytically. Although experiments can yield the most realistic results, they can become very expensive and time consuming, requiring test article fabrication and elaborate instrumentation. While the simplified analytical approach described in section VI.A has solid historical precedence and it yield rapid and useful results, it is nevertheless desired to quantify the effect of non-ideal features (e.g., internal structure, simplifying assumptions) with more recent tools such as CFD (Computational Fluid Dynamics), which is a relatively low-cost, less time-consuming, and high fidelity approach. Detailed tank geometries can be directly imported into a CFD model, and simulations can be configured and run in a reasonable amount of time. The only drawback to using CFD is that it is numerically complex and due diligence must be taken in conducting independent studies to validate its results over a range of applicable configurations.

In the Altair tank slosh study, slosh frequencies were obtained through the commercially available CFD code, Flow3D.™ The Flow3D™ code is an optimal choice for modeling tank slosh in that it implements a Volume of Fluid (VOF) algorithm to accurately predict the shape of free surfaces of fluids. A CAD model of the internal volume of the tank was directly imported into the CFD model and a Cartesian grid was created to discretely resolve the fluid area into 2 cm × 2 cm × 2 cm elements. Two models were created and run for each tank, one with the internal structure and one without it, in order to observe the effects of the structure on the slosh frequency. The resulting initial configurations for the LH2 tank and LO2 tank (with internal structure) are shown in Figure 11a and Figure 11b, respectively.

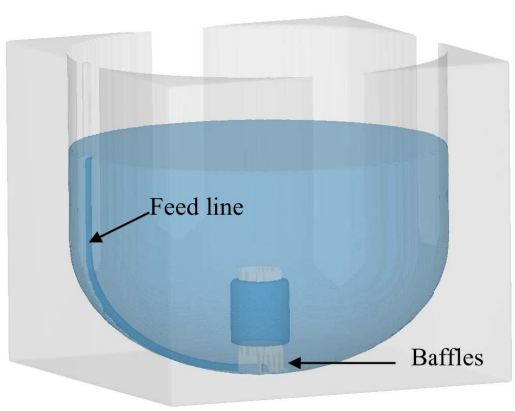

Figure 11a: Altair LH2 tank in Flow3D™

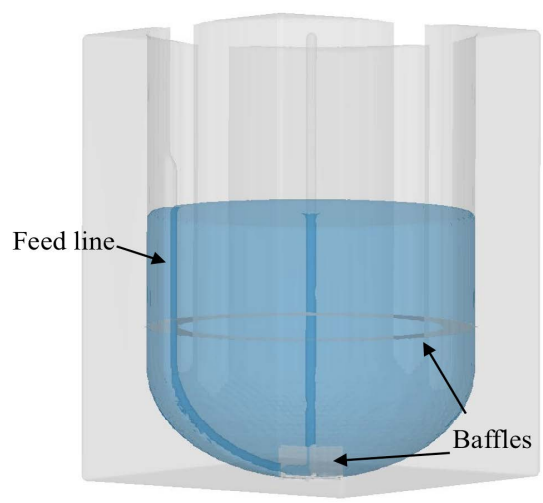

Figure 11b: Altair LO2 tank in Flow3D™

Fill fraction and acceleration were then defined for each significant event in the mission profile and a slosh simulation was run for each. These events were listed in Table 3.

In order to get the fluid moving, a lateral force of 0.5 m/s^2 was imparted laterally on the tank for 2 s, then stopped, causing the fluid to oscillate at its natural frequency in the direction of excitation. The simulations were run for 80 seconds and fluid heights at the walls in the plane of excitation were recorded to obtain wave heights as a function of time. These values were then exported to Matlab© where an FFT was performed on the data to obtain the slosh frequency. The results are depicted in Fig. 12 and also highlight the minimal dependence of the frequency on the presence of this particular internal structure. The bare tank values were then compared to the simplified analytical results of Figure 9. The natural frequencies predicted by the two approaches matched each other very closely.

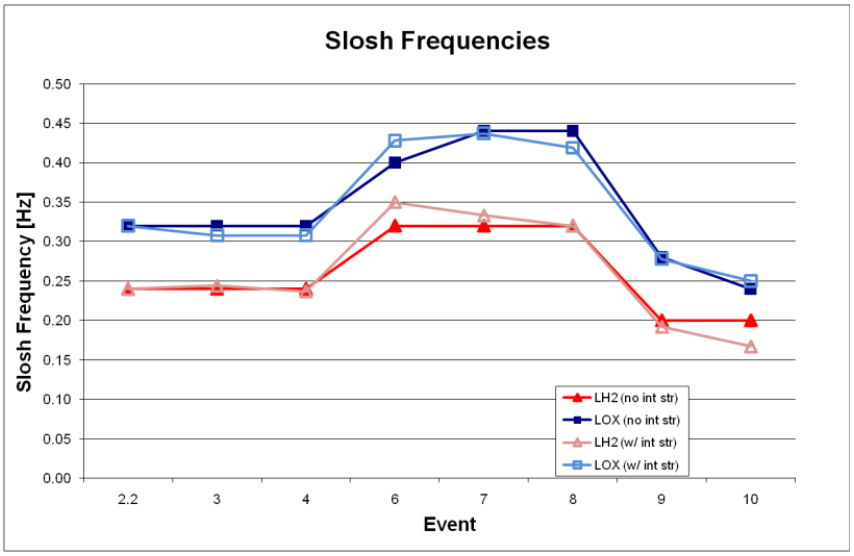

Figure 12. CFD Slosh Frequencies (events are defined in Table 3 and caption of Fig. 9)

In order to verify the validity of the Flow3D™ results, an independent anchoring exercise was performed, where Flow3D™ was used to model a simple tank configuration, for which the geometry, fill heights and experimentally obtained slosh frequencies were clearly defined and documented. In the experiment selected,[32] a 192-mm diameter tank was filled with water to various levels, ranging from 30 to 150 mm, and laterally excited to obtain frequency. This configuration was modeled in Flow3D™ and the process that was used to obtain the Altair tank slosh frequencies was repeated. The results are shown in Fig. 13. According to this exercise, Flow3D™ tends to overestimate the slosh frequencies by 7–14%. However, slosh test experience has shown that the specific methodology adopted for data reduction (i.e., excitation method, force vs. wave height trace, etc.) can affect the reported natural frequency by similar margins. This correlation, along with the favorable comparison with the Apollo-vintage methodology, is considered satisfactory confirmation of the accuracy of the Flow3D™ prediction. Other slosh parameters, such as damping ratio, pendulum length, slosh mass, etc., can also be obtained through CFD using a similar method, but work is required to experimentally validate the values of each.

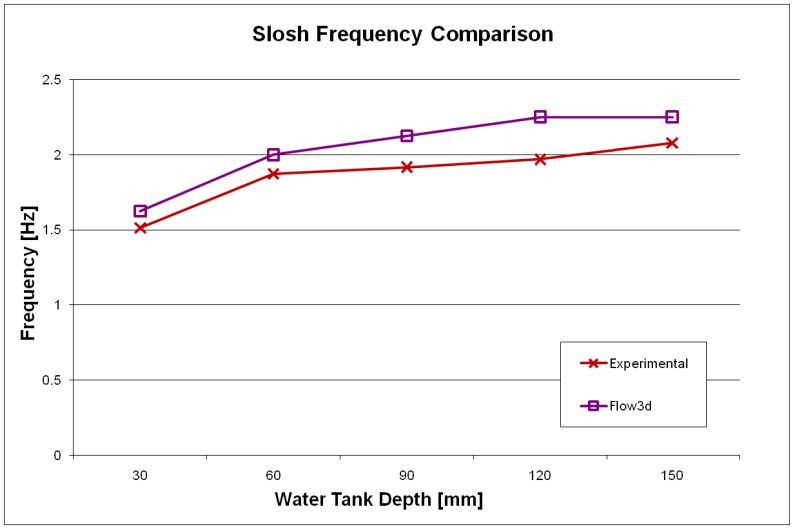

Figure 13. Results of CFD Slosh Anchoring Exercise

VII. Some Preliminary Thought on the Altair Thrust Vector Control Design

Thrust vector control of a spacecraft in a powered flight is in general quite challenging. This is because the TVC controller must compensate for a broad range of system dynamics (e.g., fuel slosh) some of which are poorly damped and others might have frequencies that are relatively close to the natural frequency of the total system. There are two obvious issues associated with controlling a spacecraft in a powered burn with propellant sloshing. First, the TVC control engineer must consider the amount of mechanical passive damping that might be needed. The second issue is related to the separation between the TVC controller bandwidth (BW) and the slosh mode frequency.

As discussed in section VI.A.3, damping ratio of fuel slosh is a function of fuel tank geometry, longitudinal acceleration, and kinematic viscosity of the propellant. Estimated values of achieved damping ratios of Apollo fuel slosh modes are on the order of 0.1–0.16%.[30] Using available empirical formulae,[24] Altair GN&C team estimated the damping ratios of fuel slosh modes in a *clean* cylindrical tank (cf. Table 4). These estimates indicate that Altair fuel slosh damping ratios are even lower than those of Apollo's tanks. Baffles for the Altair's fuel tanks on both the ascent and descent modules will be needed. Baffles of various configurations add passive damping to the sloshing fuel. Damping ratios of 1–5% is achievable via baffles.[35] The obvious penalties of baffles are the weight increase and the manufacturability of tanks with baffles. Compartmentation of a tank will, in general, increase the slosh mode frequency. This is the case because, in general, slosh mode frequency is inversely proportional to the square-root of the tank characteristic dimension (cf. Eq. (6)). Again, there will be a weight penalty.

The type of slosh controller that is needed to stabilize fuel sloshing during a powered burn depends on the degree of passive damping afforded by baffles.[19] Also, if the slosh mode frequency is significantly larger than the TVC controller BW, a gain stabilization of the slosh mode could be achieved via a roll-off filter. Else, the control engineer will have to use phase-lead filter to stabilize the slosh mode dynamics. To this end, the sloshing modes must be characterize with accuracy and the phase-lead filter carefully designed taking into consideration the dynamics of the gyroscope, gimbal actuator, and other nonlinearities.

There is a general desire to select the TVC bandwidth as large as possible, not only to minimize maneuver errors (cf. Section IV.C) but also to keep both the spacecraft rate and the corresponding engine gimbal rate to within acceptable levels at ignition. Larger bandwidth will also help to bound the magnitude of the gimbal excursion angle at ignition (see Table 5, a representative engine gimbal excursion budget). The ratio of slosh mode frequency to BW of the Apollo TVC systems was ≈2.[20] That for the space shuttle TVC system was 1.94.[21] As depicted in Fig. 9, Altair's slosh mode frequencies vary over a range of 0.21–0.44 Hz from LOI to touchdown. Based on the general guideline of maintaining a 2:1 ratio between the fundamental slosh mode frequency and the TVC BW, the Altair GN&C team picked a placeholder TVC bandwidth of 0.12–0.15 Hz. This selection is comparable with the bandwidths used by Apollo, which was 0.13–0.18 Hz.[20] The TVC bandwidth of the space shuttle was 0.13 Hz.[21] Note that the selected TVC BW is also more than an order of magnitude lower than all other system dynamics and "flexibilities" including the engine gimbal actuator bandwidth, sensor bandwidth, structural frequency, the "tail-wags-dog" spacecraft-engine interaction frequency,[27,31,38] and others (see also Fig. 14).

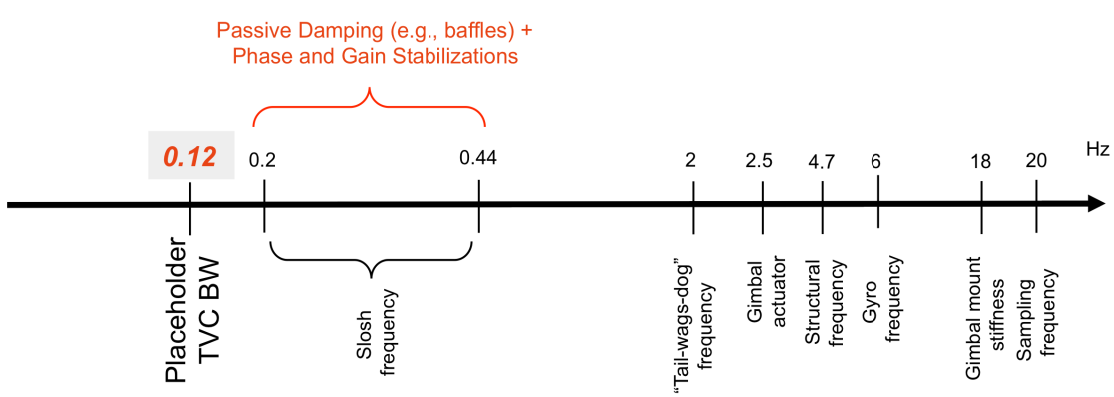

Figure 14. Placeholder TVC Bandwidth Relative to Slosh and Other System Dynamics.

The placeholder TVC controller bandwidth wasn't selected based solely on the slosh mode frequency. The TVC control engineer must also consider sets of performance and stability requirements. A representative TVC performance requirement is the time it takes the control system to respond and settle to within ±5% of an attitude command. Representative stability requirements are the commonly-used gain and phase margins of a control system. To evaluate the compatibility of the placeholder TVC BW with time-domain performance requirements, let us consider the simplified block diagram of the Altair TVC control loop depicted in Fig. 15.

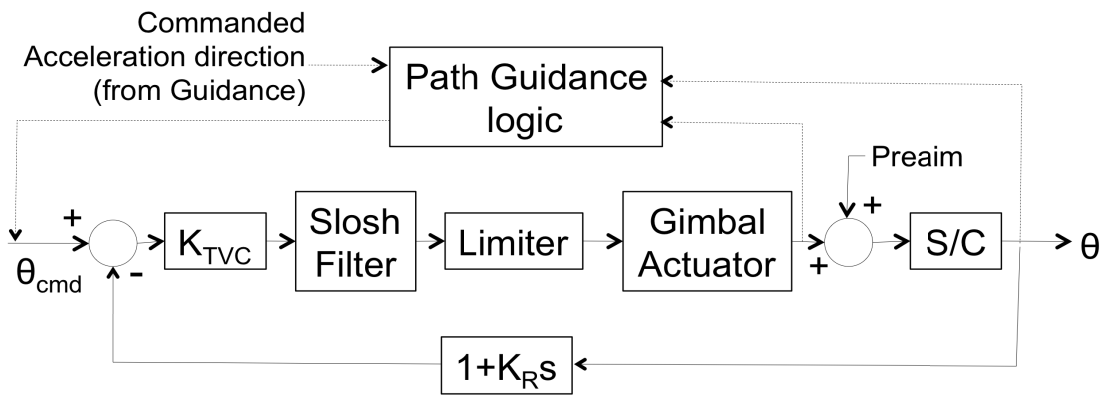

Figure 15. A Conceptual Block Diagram of the TVC Control Loop

The control loop consists of two components, the outer path guidance loop and the inner attitude control loop.[19,21,27,35] The bandwidth of the outer loop is typically low when compared with the inner loop's bandwidth. The function of the inner loop is to achieve the S/C attitude command generated by the outer guidance loop, in the presence of fuel sloshing, structural dynamics, engine gimbal actuators' nonlinearities, and other system disturbances. The function of the outer loop is to respond to the acceleration command that is computed onboard by the guidance algorithm. The interactions between guidance and control were discussed in Ref. 6. The focus of this paper is on the inner attitude control loop. Discussions on the path guidance loop design were also given in Refs. 19, 21, 27, and 35.

In Fig. 15, the S/C is modeled as a rigid body with slosh and structural dynamics. A representative transfer function of the S/C with rigid-body and slosh dynamics was given in Eq. (2). The magnitudes of Altair's gain factor K (cf. Eq. (2)), at the start and end of the PD&L phase, are approximately 0.323 and 0.379 s^{-2}, respectively. The block labeled "gimbal actuator" represents an electro-mechanical control system with multiple nonlinearities such as backlash, hysteresis, and hard stop. The block labeled K_{TVC} denotes the feed-forward gain. The bandwidth of the TVC control loop, in Hz, is Ω_{TVC} given in Eq. (8).

$$\Omega_{TVC} = \frac{\sqrt{K_{TVC}K}}{2\pi}$$
$$\xi_{TVC} = \frac{1}{2}K_R\sqrt{K_{TVC}K} \tag{8}$$

To maintain a constant TVC bandwidth throughout the PD&L burn, there will be a need to *gain schedule* K_{TVC} to compensate for the variation in the gain factor K during the PD&L burn. For example, to achieve a constant BW of 0.12 Hz, K_{TVC} must be 1.76 and 1.50 [-] at the start and end of the PD&L burn, respectively.

The type of slosh filter (notch filter, phase-lead, or roll-off) needed depends on the separation between the slosh mode frequency and the TVC BW. If the slosh mode frequency is significantly larger than the bandwidth, a 2nd order roll-off filter might suffice to remove any undesirable interactions between the slosh mode and the control of the spacecraft rigid body mode. Else, a phase-lead filter might be needed. The block labeled "limiter" is used to limit the gimbal angle command generated by the slosh filter to a level that could be supported by the gimbal actuator (see also Table 5). Finally, in the feedback path, we note the use of attitude rate feedback to add "damping" to the control loop. The resultant damping ratio of the TVC control loop (ξ_{TVC}) is given in Eq. (8). To achieve a damping ratio of $1/\sqrt{2}$ and a constant BW of 0.12 Hz throughout the PD&L burn, K_R must assume a constant value of 1.88 s.

If all the high-frequency dynamics (slosh, structure, gimbal, gyroscope, etc.) and nonlinearities of the TVC control loop depicted in Fig. 15 are neglected, one can derive closed-form expressions for the time histories of the S/C's attitude (and the corresponding gimbal angle) when the TVC controlled loop is subjected to a step change in the gimbal angle ε (e.g., due to a mispointed engine at ignition). In the special case when $\xi_{TVC}=1/\sqrt{2}$, the peak S/C's attitude and rate, as well as the peak gimbal angle and rate are given by expressions of Eq. (9).

$$
\begin{aligned}
&\varepsilon\,[\text{rad}] = \text{Gimbal mispointing error}\\
&\xi = \text{ Damping ratio } = \frac{1}{\sqrt{2}}\\
&\text{Peak S/C rate [rad/s]} \approx \varepsilon\sqrt{\frac{K}{K_{TVC}}}e^{-\frac{\pi}{4}}\\
&\text{Peak S/C angle [rad]} \approx \frac{\varepsilon}{K_{TVC}}[1+e^{-\pi}]\\
&\text{Peak gimbal rate [rad/s]} \approx \varepsilon\sqrt{2KK_{TVC}}\\
&\text{Peak gimbal angle [rad]} \approx \varepsilon(1+e^{-\frac{\pi}{2}})
\end{aligned}
\tag{9}
$$

According to Eq. (9), for a TVC control system with a 0.12-Hz bandwidth and a gimbal angle step size of 1°, the peak S/C's attitude and rate are 0.6° and 0.2 °/s, respectively. Note that this peak Altair's attitude rate, 0.2 °/s, is comparable to the peak rate experienced by Apollo-11 at PDI, which was 0.25 °/s. The computed peak gimbal angle and rate of Altair are 1.21° and 1.07 °/s, respectively. Note that the peak Altair's gimbal rate is lower than the peak gimbal rate experienced by Apollo-11 at the start of its Trans-Earth Insertion (TEI) burn, which was 2 °/s. The peak gimbal angle of Altair, 1.21°, represents about 20% of the ±6° engine gimbal angle excursion range, and is deemed acceptable. In the representative engine gimbal angle budget given below (Table 5), 1.5° was allocated for the peak gimbal excursion at burn ignition.

The gain and phase margins selected for the Apollo TVC designs were 8–9 dB and 47°, respectively.[20] The gain and phase margins of space shuttle TVC designs were 8–18 dB and 30-50°, respectively.[21] Guided by these selections, the placeholder stability margins for the Altair TVC controller are: Gain margin ≥ 9 dB, and phase margin ≥45°.

In the nominal DRM, the gimbaled engine of the descent module will be used to perform three burns:

- Lunar orbit insertion (LOI) burn of the mated Orion/Altair vehicle,
- Plane change (PC) ΔV burn of the Altair vehicle, and
- Powered descent and landing (PD&L) burn of the Altair vehicle.

The c.m. of the spacecraft (either the mated Orion/Altair vehicle or Altair alone) changed significantly from the LOI burn to the PD&L burn. Since the engine thrust vector must point through the c.m. locations of the vehicle during these burns, it is important to ascertain that the currently assumed excursion range of the engine gimbal actuators, ±6° per axis, is adequate. To this end, a preliminary budget of the engine gimbal angle is given in Table 5.

The c.m. locations of the mated Altair/Orion vehicle (at the start and end of the LOI burn) and Altair (at the start and end of the PD&L burn) were estimated by the Altair vehicle engineering team. Using these estimates, one can

compute the angles between the pointing vectors (from the engine pivot to the vehicle's c.m.) and the spacecraft's X-axis. Results are given in Fig. 16. Let's first focus on the left figure of Fig. 16 which assumed uniform flow of the propellants (all eight propellant tanks are drained perfectly evenly). Note that the two bounding pointing vectors are the one at the start of the LOI burn and that at the start of the PD&L burn. The angular range between these bounding vectors is 4.74°. The tentative plan is to cant the descent engine at the mid-point of this excursion range. The resultant cant angle, between the null axis of the descent engine and the spacecraft's X-axis, is 3.27° (4.74°/2+0.9°). The gimbal angle at LOI ignition will be 2.37° (3.27°-0.9°). The gimbal angle at PD&L ignition will be -2.37° (3.27°-5.64°). That is, 2.37° must be budgeted to account for changes in c.m. location of the spacecraft.

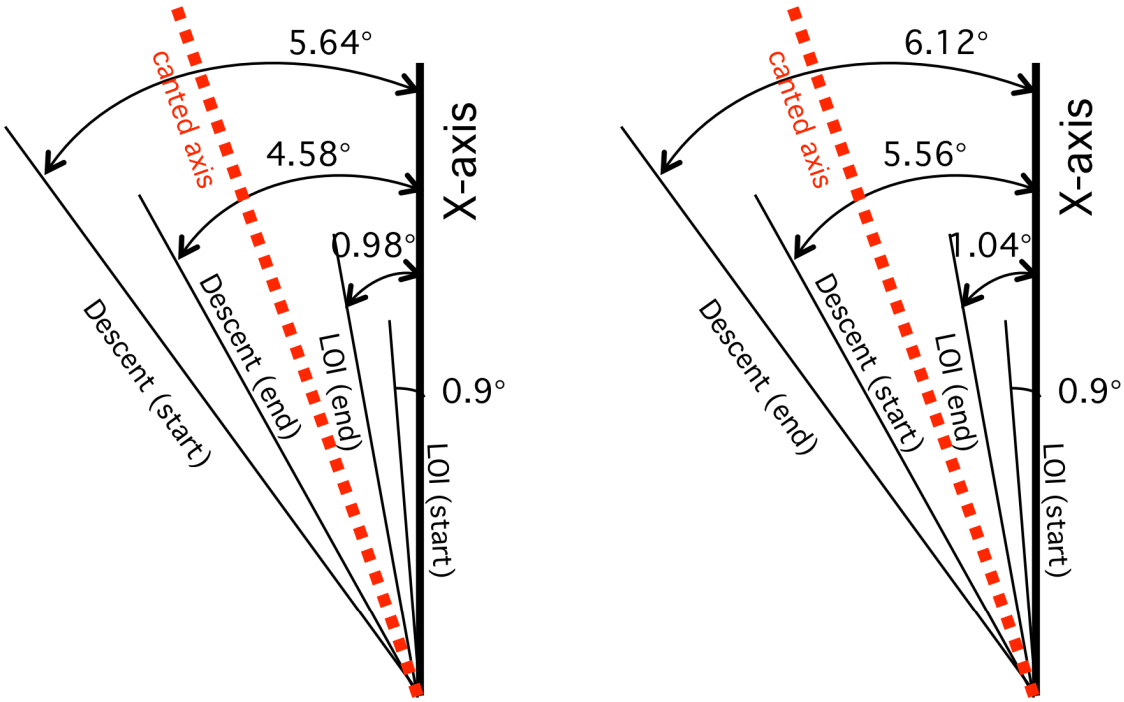

Figure 16. Pointing Vectors at LOI and PD&L Burns

(Left: Assumed Even Tank Drainage and Right: Assumed Uneven Tank Drainage)

In practice it is not possible to drain all eight propellant tanks perfectly evenly. As a result, there will be budget allocations for non-usable residual propellant as well as for c.m. shift inaccuracy associated with the location of those residuals. A fluid analysis was conducted to estimate these allocations from both deterministic and probabilistic standpoints. The deterministic case employed the latest Altair propulsion subsystem design, coupled with typical flow coefficient for all affected components. The Monte-Carlo probabilistic estimate assumed that all flow coefficient were known to within 20% (3σ). Given the symmetry of the design in the liquid side, it was found that all deterministic propellant flow distributions were caused by the pressurant-side non-symmetric plumbing, and these caused 1% propellant residuals, compared with 3.1% residuals for the probabilistic case. Assuming non-uniform flow, the pointing vectors for the LOI and PD&L burns are depicted in the right figure of Fig. 16. With non-uniform propellant flow, we note that the cant angle between the null axis of the descent engine and the spacecraft's X-axis should be 3.51° (5.22°/2+0.9°). The gimbal angle at LOI ignition will be 2.61° (3.51°-0.9°). The gimbal angle at PD&L ignition will be -2.61° (3.51°-6.12°). That is, the gimbal angle excursion range is 3.51±2.61°. If the cant angle is determined assuming uniform propellant flow, the cant angle selection error will have a deterministic component of 0.24° (3.51°-3.27°) and another probabilistic component of 0.24° (2.61°-2.37°). These

errors are captured in Table 5, the DM engine gimbal excursion budget for the PD&L burn. For brevity, the gimbal angle excursion budget for the LOI burn is not given because it is the worst case.

Table 5. Representative DM Engine Gimbal Excursion Budget at PD&L

Deterministic Gimbal Angles	Per-axis [°]
Gimbal angle from the canted null axis to vehicle's c.m. at the start of the PD&L burn	2.37
Error in the selection of the cant angle (due to assuming even propellant drainage)	0.24
Subtotal (Deterministic Error Sources)	2.61
Probabilistic Gimbal Angle Uncertainties	3σ per-axis [°]
Imperfections of the engine gimbal actuation system: Backlash, hysteresis, engine mount compliance, and others	1.0
Error in the prediction of the vehicle's c.m. location	1.0
Misalignment due to thermal mechanical instability of spacecraft structure	0.25
Error in the canting of the null axis of the DM engine gimbal system	0.50
Gimbal angle uncertainty due to c.m. shift (due to assuming even propellant drainage)	0.24
Gimbal angle uncertainty due to c.m. shift caused by sloshing motion	0.50
Peak TVC gimbal angle transient excursion (at ignition)	1.5
RSS Subtotal (Probabilistic Error Sources)	2.21
Total	4.82
DM engine gimbal excursion range	6.0

Note that, in Table 5, we have allocated 1.5° for the peak engine gimbal excursion due to TVC control transient at ignition. The peak gimbal angle excursion estimated for a TVC controller with a 0.12-Hz BW and a damping rate of 0.707 was 1.21° (cf. Eq. (9)). The allocation for gimbal angle due to prediction error of the vehicle's c.m. location is 1°. Since the distance between the engine pivot and the vehicle's c.m. is about 1.3 m at the start of the PD&L burn, 1° corresponds to about 2.3 cm knowledge error of the vehicle's c.m. location in the [Y,Z] plane. Based on this gimbal angle excursion budget for the PD&L burn and a similar one constructed for the LOI burn, the Altair GN&C team concluded that the current placeholder gimbal excursion range of ±6° is adequate. The gimbal angle excursion ranges of the LEM descent engines of Apollo-9, 10, 11, and 12 are all ±6°.The pitch and yaw gimbal angle excursion ranges of the space shuttle are ±7° and ±8°, respectively.[21]

VIII. Operations Considerations

Several operational procedures have been considered by the Altair GN&C team to minimize the impacts of fuel slosh dynamics on TVC performance. They include:

- A small ullage burn will be performed using RCS thrusters just before all engine burns performed in a "micro-g" environment (e.g., the LOI and the PD&L burns). This burn will force the fuel to the bottoms of the tanks and will make the vehicle's c.m. more predictable. The burn will also ensure that the propellant will be at the intake location at the bottom of the tank as large propellant tanks will not have micro-g fluid acquisition systems (unlike the RCS propellant tanks). No such ullage burn is needed before the Lunar ascent burn because the vehicle isn't in a micro-g environment before the ascent insertion burn. Ullage burns were used by all Apollo missions.
- After the ullage burn, engine gimbal actuators will aim the 2-dof engine axis through the predicted c.m. location of the spacecraft. This practice will minimize the disturbance experienced by the fuel due to the rising engine thrust at ignition. At the end of the last engine burn, the engine thrust vector should have passed through the spacecraft's c.m. That c.m. location should be quite close to the c.m. location of the vehicle at the start of the next engine burn (unless a vehicle reconfiguration such as undocking had occurred between the two burns). For example, the engine gimbal angles found at the end of the PC burn should be used as initial condition for the subsequent PD&L burn. "Pre-aiming" of the 2-dof engine was used by Cassini for more than 100 engine ΔV burns.[3,12]

- To avoid exciting fuel sloshing motions, "gentle" rate and acceleration profiles will be used, when possible, to slew the vehicle (e.g., for the "window-up" motion) before the start of the gimbaled engine burn. However, powered flight maneuvering late in the PD&L burn, either as part of a possible approach phase landing re-designation maneuver, or as a result of direct piloting input, may demand more substantial angular accelerations, a significant demand when sloshing vulnerability may also be substantial. For reference, the Apollo LM provided ~10 °/s^2 during this mission sub-phase.
- Use of small RCS controller deadband. During the powered descent phase of Apollo-11, the vehicle pitch rate started to diverge near PDI (at 102:36:57 MET). At that time, the peak-to-peak pitch rate was 0.6 °/s. It became 3.0 °/s when MET was 102:39:00. At MET = 102:39:30, the pitch-up maneuver was executed at the start of the approach phase, together with a throttle down and a tightening of deadband (from ±1° to ±0.3°). These control actions arrested the divergence of pitch rate (the peak-to-peak pitch rate dropped from 3.0 to 2.2 °/s).[16] The current plan is to use X-axis RCS controller deadbands of ±1°, ±0.2°, and ±0.2° during the Braking, Approach, and Terminal sub-phases of the PD&L burn.[6]

IX. Summary and Conclusions

In this paper, we described a conceptual TVC design for the Lunar Lander Altair, along with a discussion of the various powered flight maneuvers where it will be employed. The TVC controller must be designed to be robust relative to the significant fuel sloshing dynamics of the Altair vehicle. To this end, propellant slosh characteristics for the various mission powered flight phases were estimated. Also, since it is highly desirable to configure the vehicle to produce a stable interaction between the slosh mode and the spacecraft rigid body mode, fuel tanks on the ascent and descent modules must be placed with great care. Damping factors of Altair propellant slosh modes in clean tanks were estimated in our study. Since the estimated damping ratios are about two orders of magnitude less than that needed for TVC control stability, Altair fuel tanks are currently designed with baffles. The strong "couplings" between the TVC controller design (which is the responsibility of the GN&C team), fuel tank sizing (fuel slosh mode frequency is a strong function of tank geometry and tank sizing is the joint responsibility of the Propulsion and Structure teams), and tank placements (which is the responsibility of the Structure team) make it important for the GN&C, Propulsion, and Structure teams to collaborate closely during early design phases of Altair vehicle design. Beside meeting performance and stability requirements, TVC controller bandwidth must be selected taking into account the fuel slosh mode frequency. Moreover, one must check the compatibility of the TVC controller bandwidth with other vehicle system dynamics (such the engine gimbal actuator bandwidth, sensor bandwidth, structural frequency, sampling frequency of the flight software, etc.). In this paper, these key TVC design considerations are identified and described qualitatively. To quantify the performance of the TVC system, a simulation environment built around a flexible spacecraft base-body, which contains propellant slosh modes and other system dynamics and nonlinearities must be used. Future TVC design iterations will also address other important issues such as the interactions between the crews and the TVC, and will support the evolving reference design of the Altair vehicle and mission.

Acknowledgments

The work described in this paper was carried out by Jet Propulsion Laboratory, California Institute of Technology, under a contract with the National Aeronautics and Space Administration. Reference to any specific commercial product, process, or service by trade name, trademark, manufacturer, or otherwise, does not constitute or imply its endorsement by the United States Government or the Jet Propulsion Laboratory, California Institute of Technology. We are grateful to Mimi Aung, Melvin Flores, Erisa Hines, Wayne Lee, and Dan Turner (at Jet Propulsion Laboratory), Ellen Braden, Brian Derkowski, Clinton Dorris, Lauri Hansen, Brad Irlbeck, Brad Jones, Jonathan Lenius, Michael Machula, James McMicheal, Robert Merriam, Jacque Myrann, and Jake Sullivan (at the NASA Johnson Space Center); Kendall Brown, Jack Chapman, Larry Kos, and Tara Polsgrove (at the NASA Marshall Space Flight Center); Tim Collins and David North (at NASA Langley Research Center), for much helpful assistance over the past years. Also, we would like to thank our colleagues at JPL, Edward Wong and Siamak Sarani, senior members of technical staff (of the Guidance, Navigation and Control section of JPL), for their reviews and comments on an earlier version of this paper.

References

[1]Hubert, C., "Behavior of Spinning Vehicles With Onboard Liquid," Proc. 2003 Flight Mechanics Symposium, NASA, Goddard, MD 2003, pp. 1–14.

[2]Slabinski, V., "Intelsat IV in-orbit Liquid Slosh Tests and Problems in the Theoretical Analysis of the Data," in Proc. Conf. Attitude Control of Space Vehicle: Technological and Dynamical Problems Associated With the Presence of Liquids, Toulouse, France, ESA SP-129, 1977, pp. 87–102.

[3]Lee, A. Y., and Hanover, G., "Cassini Spacecraft Attitude Control System Flight Performance," *Proceedings of the AIAA Guidance, Navigation, and Control Conference, and Exhibit*, San Francisco, California, August 15–18, 2005.

[4]Ely, T., Heyne, M., and Riedel, J. E., "Altair Navigation during Trans-Lunar Cruise, Lunar Orbit, Descent, and Landing," *Proceedings of the AIAA Guidance, Navigation, and Control Conference, and Exhibi*t, Toronto, Ontario, Canada, August 2–5, 2010.

[5]Riedel, J. E., Ely, T., Lee, A. Y., Werner, R. A., Wang, T.-C., Vaughan, A. T., Nolet, S., Myers, D. M., Mastrodemos, N., Grasso, C., and David Bayard, "Optical Navigation Plan and Strategy for the Lunar Lander Altair," *Proceedings of the AIAA Guidance, Navigation, and Control Conference, and Exhibit*, Toronto, Ontario, Canada, August 2–5, 2010.

[6]Lee, A.Y., Ely, T., Sostaric, R., Strahan, A. L., Riedel, R.E., Ingham, M., Wincentsen, J., and Sarani, S., "Preliminary Design of the Guidance, Navigation, and Control System of The Altair Lunar Lander" *Proceedings of the AIAA Guidance, Navigation, and Control Conference, and Exhibit*, Toronto, Ontario, Canada, August 2-5, 2010.

[7]Kos, L., Polsgrove, T., Sostaric, R., Braden, E., Sullivan, J. J., and Le, T. T., "Altair Descent and Ascent Reference Trajectory Design and Initial Dispersion Analyses," *Proceedings of the AIAA Guidance, Navigation, and Control Conference, and Exhibit*, Toronto, Ontario, Canada, August 2-5, 2010.

[8]Strahan, A. L., and Johnson, A., "Terrain Hazard Detection and Avoidance during the Descent and Landing Phase of the Lunar Lander Altair Mission," *Proceedings of the AIAA Guidance, Navigation, and Control Conference, and Exhibit*, Toronto, Ontario, Canada, August 2-5, 2010.

[9]Sullivan, J., Lee, A. Y., and Grover, R., "Rendezvous and Docking Sensor and Effector System Designs for the Lunar Lander Altair," *Proceedings of the AIAA Guidance, Navigation, and Control Conference, and Exhibit*, Toronto, Ontario, Canada, August 2-5, 2010.

[10]Strahan, A. L., Law, H. G., Bilimoria, K. D., and Mueller, E. R., "A Review of Research Into GNC Performance and Interface Design for A Piloted Lunar Landing," *Proceedings of the AIAA Guidance, Navigation, and Control Conference, and Exhibit*, Toronto, Ontario, Canada, August 2-5, 2010.

[11]Strikwerda, T.E., et al, "NEAR Shoemaker: Major Anomaly Survival, Delayed Rendezvous, and Mission Success," in Guidance and Control 2001, San Diego, 2001, pp. 597–614.

[12]Burk, T., "Attitude Control Performance During Cassini Trajectory Correction Maneuvers," *Proceedings of the AIAA Guidance, Navigation, and Control Conference, and Exhibit*, San Francisco, California, August 15–18, 2005.

[13]Constellation Architecture Requirements Document (CARD), CxP 70000, Release Version D, 2009, Johnson Space Center.

[14]Gates, C. R., "A Simplified Model of Midcourse Maneuver Execution Errors," JPL Technical Report 32-504, Jet Propulsion Laboratory, Pasadena, California, October 15, 1963.

[15]NASA Manned Spacecraft Center, *Apollo 10 Guidance, Navigation and Control System Performance Analysis Report*, 11176-H386-R0-00, Project Technical Report, Task E-38C, NAS 9-8166, October 31, 1969.

[16]NASA Manned Spacecraft Center, *Apollo 11 Guidance, Navigation and Control System Performance Analysis Report*, 11176-H433-R0-00, Project Technical Report, Task E-38C, NAS 9-8166, December 31, 1969.

[17]NASA Manned Spacecraft Center, *Apollo 12 Guidance, Navigation and Control System Performance Analysis Report*, 11176-H524-R0-00, Project Technical Report, Task E-38C, NAS 9-8166, April 8, 1970.

[18]NASA Manned Spacecraft Center, *Apollo 14 Guidance, Navigation and Control System Performance Analysis Report*, MSC-04112 Supplement 1, Project Technical Report, Task E-38C, NAS 9-8166, January 1972.

[19]Wie, B., *Space Vehicle Dynamics and Control*, AIAA Education Series, May 1998.

[20]Smith, E. E., "Performance of Apollo Block II Thrust Vector Control Using the PGNCS (Preliminary Guidance Navigation and Control System)," NASA Internal Note MSC-EG-69-18, Manned Spacecraft Center, Houston Texas, April 8, 1969.

[21]Penchuk, A. and Croopnick, S., "Digital Autopilot for Thrust Vector Control of the Shuttle Orbital Maneuvering System," *Journal of Guidance and Control*, Vol. 6, No. 6, November-December, 1983, pp. 436–441.

[22]Lance, T. A., *Analysis of Propellant Slosh Dynamics and Generation of an Equivalent Mechanical Model for Use in Preliminary Voyager Autopilot Design Studies*, Technical Memorandum No. 33-306, Jet Propulsion Laboratory, California Institute of Technology, Pasadena, California, December 1, 1966.

[23]Enright, P., and Wong, E. C., "Propellant Sloshing Models for the Cassini Spacecraft," AIAA Paper 94-3730, 1994.

[24]Dodge, F. T., "The New "Dynamic Behavior of Liquids in Moving Containers," Southwest Research Institute, San Antonio, Texas, 2000 (this is an update of NASA SP-106 whose original authors are Norm Abramson, Douglas Michel, George Brooks and Helmut Bauer).

[25]Helmut, F., Fluid Oscillations in the Containers of a Space Vehicle and their Influence Upon Stability, NASA TR R-187, Marshall Space Flight Center, Huntsville Alabama, February 1964.

[26]Edelmann, R. and Dunn, P., *Dynamic Analysis of the LEM Flight Control System*, Grumman Aircraft Engineering Corporation. Report No. LED-500-3, re-labeled NASA-CR-117567, September 30, 1964.

[27]Enright, P. and Macala, G.A., "Attitude and Articulation Control of the CRAF/Cassini Spacecraft in the Presence of Structural Flexibilities and Propellant Slosh," *Proceedings of the 15th Annual AAS Guidance and Control Conference*, Keystone, Colorado, February 8-12, 1992.

[28]Bryson, A.E., *Control of Spacecraft and Aircraft,* Princeton University Press, Princeton, New Jersey, 1994.

[29]Chiang, R.Y., Breckenridge, W.G., and Wong, E., "Self-tuning Thruster Control for Cassini Spacecraft," *Proceedings of the AIAA Guidance, Navigation, and Control Conference*, San Diego, California, July 28-31, 1996.

[30]Smith, E. E., "Design of a Sampled Data Control System for Attitude Control of a Spacecraft During Powered Flight in a Gravity Free Environment," NASA Internal Note MSC 68-EG-06, Manned Spacecraft Center, Houston, Texas, May 7, 1968.

[31]Kopf, E.H., "A Mariner Orbiter Autopilot Design," Technical Report 32-1349, Jet Propulsion Laboratory, California Institute of Technology, January 15, 1969.

[32]Pal, N.C., Bhattachaharyya, S.K., and Sinha, P.K., "Experimental Investigation Slosh Dynamics of Liquid-filled Containers," Experimental Mechanics, Vol. 41, No. 1, March 2001, pp. 63-69.

[33]Abramson, H.N., editor, "The Dynamic Behavior of Liquids in Moving Containers.", NASA SP-106, 1966.

[34]Anon.: "Slosh Suppression. NASA Space Vehicle Design Criteria (Structures)", NASA SP-8031, 1969.

[35]Wie, B., "Thrust Vector Control Design for a Liquid Upper Stage Spacecraft," Journal of Guidance and Control, Vol. 8, No. 5, September-October 1985. pp. 566–572.

[36]Wie, B. and Bryson, A.E., Jr., "Pole-Zero Modeling of Flexible Space Structure," Journal of Guidance and Control, Vol. 11, No. 6, November-December 1988. pp. 554–561.

[37]Chapel, J.D., Schmitz, E., Sidney, W.P., Johnson, M.A., Good, P. G., Wynn, J. A., and Bayer, T., "Attitude Control Performance for MRO Aerobraking and the Initial Science Phase," AAS 07-097, 30th AAS Guidance and Control Conference, Breckenridge, Colorado, February 3-7, 2007.

[38]Enright, P., "Thrust Vector Control Algorithm Design for the Cassini Spacecraft," AIAA/AHS/ASEE Aerospace Design Conference, Irvine, California, February 16-19, 1993. AIAA paper 1993-1043.

[39]Vreeburg, J.P.B., "Spacecraft Maneuvers and Slosh Control," IEEE Control Systems, pp. 12–16, June 2005.